Mean-Field Floquet Theory for a Three-Level Cold-Atom Laser

by

Gage Harmon

A thesis submitted to the Faculty of the

University of Colorado in partial fulfillment

of the requirements for the degree of

Bachelor of Arts

Department of Physics

2022

This thesis entitled:
Mean-Field Floquet Theory for a Three-Level Cold-Atom Laser
written by Gage Harmon
has been approved for the Department of Physics

_____

Murray Holland

_____

Prof. Paul Beale

_____

Prof. Richard Green

Date _____

The final copy of this thesis has been examined by the signatories, and we find that both the content and the form meet acceptable presentation standards of scholarly work in the above mentioned discipline.

Harmon, Gage (B.A., Physics)

Mean-Field Floquet Theory for a Three-Level Cold-Atom Laser

Thesis directed by Prof. Murray Holland

My honors thesis provides a theoretical description for a lasing scheme of V-shaped three-level atoms interacting with an optical cavity. Gain is achieved by pumping sufficiently many atoms into the $^3P_1$ electronic excited state. The atom can then decay back to the ground state via emitting a cavity photon, followed by absorbing a photon from a second driving laser. Where it completes it cycle by decaying via spontaneous emission back to the ground state. Lasing is achieved if this gain exceeds the losses due to dissipation of cavity photons into free space. We study this system using mean-field equations for the coupled atom-cavity dynamics. With this, we determine the lasing threshold and the emission frequencies using a stability analysis. Furthermore, we are able to predict the lasing intensity and frequency using a mean-field Floquet method. This method shows a $U(1)$ symmetric lasing solution which is visible only in Fourier components while the total cavity field does not possess this symmetry. The non-linear nature of this open system is highlighted by its ability to form bistable lasing, non-lasing states, and a hysteresis when slowly ramping the pump power above threshold and back. Lastly, we compare our mean-field results with a second-order cumulant approach to verify our findings.

Dedication

To Leslie, Kane, Jeff, Steve, Scott, Jarrod, Simon, Murray, my friends, Sabor, and to those before and after me who have dedicated their lives to physics and the pursuit of knowledge.

Contents

Chapter

Figures

Figure

Chapter 1

Introduction and Motivation

Since its conception by Einstein in 1917 [15], the use of lasers and masers [41, 69] has revolutionized a myriad of aspects of physics and, in particular, set the foundation for the ever-growing field of quantum optics. A laser is created when a gain medium establishes optical gain within a cavity by way of population inversion between two atomic dressed states [47, 54]. Furthermore, the laser is classified as operating in a continuous mode when the output power is constant over time. To achieve continuous-wave lasing, a steady pump source is required to sustain the population inversion of the gain medium. This can be achieved by lasing between dressed states of a two-level atom [56], but population inversion between an internal excited and ground state can be difficult to maintain. To overcome this, techniques have been developed to lase without inversion [58]; for example, by driving a system where the lasing photon is emitted as part of multiphoton transition.

This allows for the study of cold-atom lasers based on more complicated level structures. With this in mind, we present a theoretical study of a cold-atom laser comprised of a cloud of cooled and trapped ytterbium-174 atoms. We start off by introducing the two fundamental light-matter interactions, followed by analytical and numerical tools in Chapter 2. In this, we will provide a physical and mathematical description of a two-level atom interacting with a classical and quantized field. Then a brief explanation of cumulants and Liouville space, which allows us to simulate large atom numbers while reducing our simulation times. In Chapter 3, we define our model and explain the lasing mechanism. After, we analyze the onset of lasing by performing a stability analysis on a non-lasing state against field fluctuations to determine the lasing threshold.

We subsequently introduce a Floquet method where we decompose the field and atomic density operator into three primary frequency components and explore a hysteresis regime. Finally, we compare our mean-field results with second-order cumulants and conclude with a summary of our work.

Chapter 2

Atom-Laser Interaction Background

2.1 Atom Interacting with a Classical Field

In this section, I give a description and derivation of a two-level atom interacting with a single monochromatic field along with the appropriate approximations. It follows similarly from [71, Chapter 5]. To model the field due to a laser we look at the electric field operator for a monochromatic field, with angular frequency ω at the position of the atom

$$\hat{E}(t) = \hat{\varepsilon} E_0 \cos(\omega t), \tag{2.1}$$

where $\hat{\varepsilon}$ is the polarization vector of the field. This removal of the field's spatial dependency is called the dipole approximation, which assumes the light field changes over length scales that are orders of magnitude larger than the size of the atom. This is generally applicable because atomic sizes are $\mathcal{O}(10^{-10}\,\mathrm{m})$ while optical wavelengths of light are $\mathcal{O}(10^{-7}\,\mathrm{m})$. It is favorable to decompose the field in terms of positive and negative rotating components

$$\hat{E}(t) = \hat{\varepsilon}\frac{E_0}{2}\left(e^{-i\omega t} + e^{i\omega t}\right) = \hat{E}^{(+)}(t) + \hat{E}^{(-)}(t). \tag{2.2}$$

We will approximate the atom to having only two states, where as a true atom has an infinite set of states. We denote these two states as the ground $|g\rangle$ and excited state $|e\rangle$. Then the energy difference between these states are $\Delta E = E_e - E_g$, and it is standard to rewrite this energy difference in terms of the reduced Planck's constant $\hbar$ and angular frequency ω. Using the de Broglie wavelength and photon energy relations we see the transition frequency is $\Delta E = \hbar\omega_a$. Defining the

zero-point energy to be halfway between the states, the atomic free-evolution Hamiltonian is

$$\hat{H}_A = \frac{\hbar\omega_a}{2}(|e\rangle\langle e| - |g\rangle\langle g|), \tag{2.3}$$

where the projection operators $|e\rangle\langle e|$ and $|g\rangle\langle g|$ represent the corresponding energy of each state. The atom-field interaction Hamiltonian under the dipole approximation becomes

$$\hat{H}_{AF} = -\hat{d}\cdot\hat{E}, \tag{2.4}$$

where $\hat{d}$ is the atomic dipole operator.

2.1.1 Dipole Operator and Parity

Let us consider the field interacts strongly with one electron of the atom, such that the dipole operator can be expressed in terms of the electron charge $q = -e$ and the electron's position in space $\vec{r}$ as

$$\hat{d} = -e\hat{r}. \tag{2.5}$$

We then use a parity argument in order to gain information about the structure of the dipole operator. The parity operator changes the sign of the position operator, thus the operator transformation is

$$\hat{\Pi}\hat{r}\hat{\Pi}^\dagger = -\hat{r}, \tag{2.6}$$

where $\hat{\Pi}$ is unitary such that $\hat{\Pi}$ and $\hat{\Pi}^\dagger$ apply the same operation (i.e., $\hat{\Pi}\hat{r} = -\hat{r}\hat{\Pi}$). We now turn to the energy basis and look at the diagonal elements of the dipole operator. Projecting $|a\rangle$ and the identity operator $\hat{\mathbb{I}} = \hat{\Pi}\hat{\Pi}^\dagger$ onto both sides of the dipole operator we see

$$\begin{aligned}
-e\langle a|\hat{r}|a\rangle &= -e\langle a|\hat{\Pi}\hat{\Pi}^\dagger\hat{r},\hat{\Pi}\hat{\Pi}^\dagger|a\rangle, \\
&= -e\langle a|(-1)^p\hat{\Pi}^\dagger\hat{r}\hat{\Pi}(-1)^p|a\rangle, \\
&= -e\langle a|(-\hat{r})|a\rangle, \\
&= e\langle a|\hat{r}|a\rangle.
\end{aligned} \tag{2.7}$$

This indicates the diagonal elements $\langle a|\,\hat{d}\,|a\rangle = 0$ for $a \in \{g, e\}$, as long as the states have different parity. Thus, the off-diagonal elements are non-vanishing and have the form

$$\langle g|\,\hat{d}\,|e\rangle = \langle e|\,\hat{d}\,|g\rangle^* . \tag{2.8}$$

This means the dipole operator couples the ground and excited states without producing any first-order energy shifts on the states. By applying the identity operator $\hat{\mathbb{I}} = |e\rangle\langle e| + |g\rangle\langle g|$ onto both sides of the dipole operator, we find

$$\hat{d} = \langle g|\,\hat{d}\,|e\rangle\,|g\rangle\langle e| + \langle e|\,\hat{d}\,|g\rangle\,|e\rangle\langle g| . \tag{2.9}$$

We can choose the phase of the dipole matrix element to be real, which allows us to write the dipole operator as

$$\hat{d} = \langle g|\,\hat{d}\,|e\rangle\,(\hat{\sigma} + \hat{\sigma}^\dagger), \tag{2.10}$$

where $\hat{\sigma} = |g\rangle\langle e|$ is the atomic lowering operator and $\hat{\sigma}^\dagger = |e\rangle\langle g|$ is the atomic raising operator; these operators correspond to the emission or absorption of a photon, respectively. The atom-field interaction Hamiltonian then becomes

$$\hat{H}_{AF} = -\langle g|\,\hat{d}\,|e\rangle \cdot \hat{E}(\hat{\sigma} + \hat{\sigma}^\dagger). \tag{2.11}$$

2.1.2 Rotating-Wave Approximation

We now look to decompose the dipole operator into positive and negative rotating components as done with the electric field in Eq. (2.2)

$$\hat{d} = \langle g|\,\hat{d}\,|e\rangle\,(\hat{\sigma} + \hat{\sigma}^\dagger) = \hat{d}^{(+)} + \hat{d}^{(-)}, \tag{2.12}$$

where $\hat{d}^{(+)} \sim \hat{\sigma}$ and $\hat{d}^{(-)} \sim \hat{\sigma}^\dagger$. If one were to solve the equation of motion for the expectation value of $\hat{\sigma}$ they would see it has the time dependence $e^{-i\omega_a t}$. Therefore, the atom-field interaction

Hamiltonian changes to

$$\begin{aligned}\hat{H}_{AF} &= -\left(\hat{d}^{(+)} + \hat{d}^{(-)}\right) \cdot \left(\hat{E}^{(+)} + \hat{E}^{(-)}\right), \\ &= -\hat{d}^{(+)} \cdot \hat{E}^{(+)} - \hat{d}^{(+)} \cdot \hat{E}^{(-)} - \hat{d}^{(-)} \cdot \hat{E}^{(+)} - \hat{d}^{(-)} \cdot \hat{E}^{(-)} \\ &- \left(e^{-i(\omega+\omega_a)t} + e^{-i(\omega-\omega_a)t} + e^{i(\omega-\omega_a)t} + e^{i(\omega+\omega_a)t}\right).\end{aligned} \tag{2.13}$$

We see that the first and last terms oscillate rapidly, while the middle two cross terms oscillate slowly. We can then invoke the rotating-wave approximation (RWA) which states

$$|\omega - \omega_a| \ll \omega + \omega_a. \tag{2.14}$$

This allows us to substitute the rapidly oscillating terms with their zero average value, which amounts to a coarse-graining on fs time scales [71]. This approximation is only valid for near resonant interactions and breaks down when the detuning is extremely large (i.e., $\Delta = \omega - \omega_a \approx \omega_a$) and for strong coupling (i.e., $\left|\langle g|\,\hat{\varepsilon}\cdot\hat{d}\,|e\rangle\, E_0/\hbar\right| \approx \omega_a$). Thus, the atom-field interaction Hamiltonian in the RWA becomes

$$\hat{H}_{AF} = -\hat{d}^{(+)} \cdot \hat{E}^{(-)} - \hat{d}^{(-)} \cdot \hat{E}^{(+)}. \tag{2.15}$$

By substituting Eq. (2.2) and Eq. (2.12) with the explicit time dependencies into Eq. (2.15) we can write

$$\begin{aligned}\hat{H}_{AF} &= -\langle g|\,\hat{\varepsilon}\cdot\hat{d}\,|e\rangle \left(E_0^{(-)}\hat{\sigma}e^{i\omega t} + E_0^{(+)}\hat{\sigma}^\dagger e^{-i\omega t}\right) \\ &= \frac{\hbar\Omega}{2}(\hat{\sigma}e^{i\omega t} + \hat{\sigma}^\dagger e^{-i\omega t}),\end{aligned} \tag{2.16}$$

where we have defined the Rabi frequency as

$$\Omega = -\frac{2\,\langle g|\,\hat{\varepsilon}\cdot\hat{d}\,|e\rangle\, E_0^{(+)}}{\hbar} = -\frac{\langle g|\,\hat{\varepsilon}\cdot\hat{d}\,|e\rangle\, E_0}{\hbar}, \tag{2.17}$$

and have assumed $E_0^{(+)}$ to be real. The Rabi frequency denotes the strength of the atom-field coupling and is proportional to the square root of the laser's intensity (i.e., $\Omega \propto \sqrt{I}$). The total Hamiltonian for a two-level atom interacting with a classical field is then

$$\hat{H}_{tot} = \hat{H}_A + \hat{H}_{AF} = \frac{\hbar\omega_a}{2}(|e\rangle\langle e| - |g\rangle\langle g|) + \frac{\hbar\Omega}{2}(\hat{\sigma}e^{i\omega t} + \hat{\sigma}^\dagger e^{-i\omega t}). \tag{2.18}$$

2.1.3 Interaction Picture

The goal of this subsection is to provide some information regarding the various pictures we deal with when studying quantum mechanics. These pictures describe whether the time dependence is carried by the state vectors $|\psi\rangle$ and or operators $\hat{O}$ and how they evolve. I then give an example using Eq. (2.18). I refer the reader to [71, Chapter 4, §2] for a more detailed discussion about the interaction picture.

We start off by considering a time-independent Hamiltonian that can be decomposed into two separate parts

$$\hat{H}_{tot} = \hat{H}_0 + \hat{H}_{int}, \tag{2.19}$$

where $\hat{H}_0$ is the free evolution term and $\hat{H}_{int}$ is the interaction term. A state vector in the interaction picture $|\psi(t)\rangle_I$ is the transformed state vector of the Schrödinger picture $|\psi(t)\rangle_S$ by the free part of the Hamiltonian

$$|\psi(t)\rangle_I = e^{i\hat{H}_0 t/\hbar} |\psi(t)\rangle_S , \tag{2.20}$$

while an operator transforms according to

$$\hat{O}(t)_I = e^{i\hat{H}_0 t/\hbar} \hat{O}_S e^{-i\hat{H}_0 t/\hbar}, \tag{2.21}$$

where $\hat{O}_S$ is an operator in the Schrödinger picture. The third picture in quantum mechanics is referred to as the Heisenberg picture, where the state vectors are time-independent and the operators are time-dependent; they are defined as

$$|\psi\rangle_H = e^{i\hat{H}_{tot} t/\hbar} |\psi(t)\rangle_S , \tag{2.22}$$

and

$$\hat{O}(t)_H = e^{i\hat{H}_0 t/\hbar} \hat{O}_S e^{-i\hat{H}_0 t/\hbar}. \tag{2.23}$$

Let us now work through an example beginning with

$$\hat{H}_{tot} = \frac{\hbar\omega_a}{2}(|e\rangle\langle e| - |g\rangle\langle g|) + \frac{\hbar\Omega}{2}(\hat{\sigma}e^{i\omega t} + \hat{\sigma}^\dagger e^{-i\omega t}). \tag{2.24}$$

This Hamiltonian is defined in the Schrödinger picture and we wish to move this Hamiltonian into the interaction picture. We do this by moving into a frame rotating with the laser frequency ω,

$$\hat{H}_0 = \frac{\hbar\omega}{2}(|e\rangle\langle e| - |g\rangle\langle g|). \tag{2.25}$$

By applying Eq. (2.21) to Eq. (2.18) we write

$$\begin{aligned}\tilde{\hat{H}}_{tot} &= e^{i\hat{H}_0 t/\hbar}(\hat{H}_{tot} - \hat{H}_0)e^{-i\hat{H}_0 t/\hbar} \\ &= -\frac{\hbar\Delta}{2}(|e\rangle\langle e| - |g\rangle\langle g|) + \frac{\hbar\Omega}{2}(e^{i\hat{H}_0 t/\hbar}\hat{\sigma}e^{-i\hat{H}_0 t/\hbar}e^{i\omega t} + h.c.),\end{aligned} \tag{2.26}$$

where we have defined the detuning $\Delta = \omega - \omega_a$. We now calculate the transformation of the atomic lowering operator from the Schrödinger picture into the interaction picture,

$$\tilde{\hat{\sigma}} = e^{i\hat{H}_0 t/\hbar}\hat{\sigma}e^{-i\hat{H}_0 t/\hbar}. \tag{2.27}$$

Taking the time derivative of Eq. 2.27 and using the fact that $\hat{H}_0$ commutes with itself we arrive at

$$\frac{d\tilde{\hat{\sigma}}}{dt} = \frac{i}{\hbar}\Big(e^{i\hat{H}_0 t/\hbar}\Big[\hat{H}_0, \hat{\sigma}\Big]e^{i\hat{H}_0 t/\hbar}\Big), \tag{2.28}$$

where $[\hat{A}, \hat{B}] = \hat{A}\hat{B} - \hat{B}\hat{A}$ is the commutator of two operators. After performing the necessary algebra we arrive at the following differential equation

$$\frac{d\tilde{\hat{\sigma}}}{dt} = -i\omega\tilde{\hat{\sigma}}. \tag{2.29}$$

Upon taking the limits of integration to be from 0 to t and solving the differential equation by separation of variables we obtain

$$\tilde{\hat{\sigma}} = \hat{\sigma}e^{-i\omega t}, \tag{2.30}$$

where we have set the initial condition $\hat{\sigma}(t = 0) = \hat{\sigma}$. Applying the same process to the atomic raising operator $\hat{\sigma}^\dagger$ we would get the Hermitian conjugate of Eq. (2.30). As we can see, the atomic lowering operator in the interaction picture picks up an exponential with the frequency of the rotating frame. Substituting these operators back into Eq. (2.18) we arrive at the interaction picture Hamiltonian for a two-level atom interacting with a classical field under the RWA and dipole approximation:

$$\tilde{\hat{H}}_{tot} = -\frac{\hbar\Delta}{2}(|e\rangle\langle e| - |g\rangle\langle g|) + \frac{\hbar\Omega}{2}(\hat{\sigma} + \hat{\sigma}^\dagger). \tag{2.31}$$

2.1.4 Density Operator

The state vector $|\psi\rangle$ describes the state of a quantum system, but is limited to only representing pure states. For example, one could not write down the state vector for a mixed ensemble of atoms, where a fraction of the atoms are characterized by $|\alpha\rangle$ and the other fraction by $|\beta\rangle$. This calls for the need for a more general object to represent the state of a quantum system, especially for quantum systems that interact with an external system whose evolution is unknown. The density operator for a mixed ensemble is defined as [64]

$$\hat{\rho} = \sum_i w_i \left|\psi_i\right\rangle \left\langle\psi_i\right|, \tag{2.32}$$

where $|\psi_i\rangle$ is the set of states a system can be in. The density operator describes the statistical state of a quantum system and can represent both pure and mixed states. We do not explicitly know what state the system is in but rather we assign a probability or population w_i to the state $|\psi_i\rangle \langle\psi_i|$. When taking the trace of the density operator the fractional populations must satisfy the normalization condition

$$\mathrm{Tr}(\hat{\rho}) = \sum_i w_i \langle\psi_i|\psi_i\rangle = 1. \tag{2.33}$$

It is also important to note the density operator is Hermitian and completely positive. We are interested in how a quantum system evolves in time, strictly speaking how the density operator changes as a function of time. By taking the time derivative of the density operator and utilizing the Schrödinger equation $i\hbar\partial_t |\psi\rangle = \hat{H} |\psi\rangle$, we can derive the equation of motion for the density operator under unitary time evolution:

$$\begin{aligned}
\partial_t\hat{\rho} &= \frac{1}{i\hbar}\sum_i w_i\Big[\big(\partial_t |\psi_i\rangle\big)\langle\psi_i| + |\psi_i\rangle\big(\partial_t \langle\psi_i|\big)\Big] \\
&= \frac{1}{i\hbar}\sum_i w_i\big(\hat{H}|\psi_i\rangle\langle\psi_i| - |\psi_i\rangle\langle\psi_i|\hat{H}\big) \\
&= \frac{1}{i\hbar}\big[\hat{H},\hat{\rho}\big].
\end{aligned} \tag{2.34}$$

The expression above is the Schrödinger–von Neumann equation. However, Eq. (2.34) only encapsulates the coherent or reversible dynamics a system will undergo and does not take into account

any dissipative processes. In this thesis we want to investigate the dynamics of open quantum systems, that is when a quantum system couples to an external quantum system whose evolution we do not directly track. In order to study the evolution of open quantum systems we choose to use the Born–Markov master equation

$$\partial_t \hat{\rho} = \hat{\mathcal{L}} \rho, \tag{2.35}$$

where $\hat{\mathcal{L}}$ is the Liouvillian superoperator. The term superoperator comes from the fact that the Liouvillian is a higher-dimensional object and operates from both sides of the density operator. Eq. (2.35) is a compact form of the master equation, one can express the full master equation as

$$\partial_t \hat{\rho} = \frac{1}{i\hbar}\big[\hat{H}, \hat{\rho}\big] + \sum_k \big(\hat{J}_k \hat{\rho} \hat{J}_k^\dagger - \frac{1}{2}\hat{J}_k^\dagger \hat{J}_k \hat{\rho} - \frac{1}{2}\hat{\rho}\hat{J}_k^\dagger \hat{J}_k\big), \tag{2.36}$$

where the first term is the Schrödinger–von Neumann equation and the second term is the sum of Lindblad superoperators with corresponding jump operator $\hat{J}_k$. The Lindblad superoperator is able to encapsulate the dissipative dynamics of an open quantum system, such as spontaneous emission, dephasing, inhomogeneous broadening, and more. These effects are represented by an operator and decay rate, which we call jump operators.

2.2 Atom Interacting with a Quantized Field

In this section, I go over the quantization of a single-mode field and give an example of a two-level atom interacting with a quantized field of a cavity known as the Jaynes–Cummings model. I follow the methods prescribed in [21, Chapter 2] and [71, Chapter 8].

2.2.1 Field Quantization of a Single-Mode

Many systems we are interested in involve a quantized field interacting with atoms inside a cavity. Often there is only one resonant mode within the cavity; here we show how to treat a single-mode quantum mechanically. We start by introducing the canonically conjugate variables q and p, where q is the canonical position and p is the canonical momentum. Now, consider a monochromatic field with frequency ω inside a cavity with perfectly reflecting mirrors where the

field is polarized along the x-direction:

$$\vec{E}(z,t) = \hat{x}\sqrt{\frac{2\omega^2}{V\varepsilon_o}}q(t)\sin(kz), \tag{2.37}$$

where V is the effective mode volume (length of cavity $\times$ (beam waist)^2), ω is the oscillation frequency of the field, k is the wave number, and $q(t)$ is the dimensionless amplitude of the field. The wave number can be related to the frequency by $\omega = kc$. The field must obey Maxwell's equations in a vacuum with no charge or current:

$$\vec{\nabla} \times \vec{E} = \partial_t \vec{B}, \tag{2.38}$$

$$\vec{\nabla} \times \vec{B} = \frac{1}{c^2}\partial_t \vec{E}, \tag{2.39}$$

$$\vec{\nabla} \times \vec{E} = 0, \tag{2.40}$$

$$\vec{\nabla} \times \vec{B} = 0. \tag{2.41}$$

Substituting Eq. (2.37) into Eq. (2.39), the magnetic field in the cavity is

$$\vec{B}(z,t) = \frac{\hat{y}}{c^2 k}\sqrt{\frac{2\omega^2}{V\varepsilon_0}}\dot{q}(t)\cos(kz), \tag{2.42}$$

where $\dot{q}(t) = p(t)$. We can now write the total energy density as the sum of the electric and magnetic energy density

$$U = \frac{1}{2}(\varepsilon_o E^2 + \frac{1}{\mu_o}B^2), \tag{2.43}$$

and then the classical Hamiltonian is just the energy density over the entire volume

$$H = \frac{1}{2}\int_V (\varepsilon_o E^2 + \frac{1}{\mu_o}B^2)dV. \tag{2.44}$$

After carrying out the integral it can be shown that

$$H = \frac{1}{2}(p^2 + \omega^2 q^2), \tag{2.45}$$

and this is equivalent to the Hamiltonian of a classical harmonic oscillator of unit mass. To make the transition from classical variables to quantum operators we replace q and p with their operator equivalents $\hat{q}$ and $\hat{p}$. These operators must satisfy the canonical commutation relation

$$\left[\hat{q}, \hat{p}\right] = i\hbar. \tag{2.46}$$

Then the electric and magnetic fields become the operators

$$\hat{E}(z,t) = \hat{x}\sqrt{\frac{2\omega^2}{V\varepsilon_o}}\hat{q}(t)\sin(kz) \tag{2.47}$$

and

$$\hat{B}(z,t) = \hat{y}\frac{1}{c^2k}\sqrt{\frac{2\omega^2}{V\varepsilon_0}}\hat{p}(t)\cos(kz), \tag{2.48}$$

respectively. The Hamiltonian becomes

$$\hat{H} = \frac{1}{2}(\hat{p}^2 + \omega^2\hat{q}^2). \tag{2.49}$$

We now introduce the non-Hermitian operators $\hat{c}$, the annihilation operator which represents the destruction of a photon, and $\hat{c}^\dagger$, the creation operator which represents the creation of a photon. They can be expressed in terms of the Hermitian operators $\hat{q}$ and $\hat{p}$ as

$$\hat{c} = \frac{1}{\sqrt{2\hbar\omega}}(\omega\hat{q} + i\hat{p}), \tag{2.50}$$

and

$$\hat{c}^\dagger = \frac{1}{\sqrt{2\hbar\omega}}(\omega\hat{q} - i\hat{p}). \tag{2.51}$$

The electric and magnetic field operators then become

$$\hat{E}(z,t) = \hat{x}\sqrt{\frac{\hbar\omega}{V\varepsilon_o}}(\hat{c} + \hat{c}^\dagger)\sin(kz), \tag{2.52}$$

and

$$\hat{B}(z,t) = -i\hat{y}\frac{\mu_o}{k}\sqrt{\frac{\varepsilon_o\hbar\omega^3}{V}}(\hat{c} - \hat{c}^\dagger)\cos(kz). \tag{2.53}$$

Since the operators $\hat{c}$ and $\hat{c}^\dagger$ are non-Hermitian they have the following commutation relation

$$\left[\hat{c}, \hat{c}^\dagger\right] = 1, \tag{2.54}$$

and, as a result, the Hamiltonian operator takes the form

$$\hat{H} = \hbar\omega\Big(\hat{c}^\dagger\hat{c} + \frac{1}{2}\Big). \tag{2.55}$$

As we can see this is the same Hamiltonian for a one-dimensional quantum harmonic oscillator, an interesting correspondence nonetheless.

2.2.2 Jaynes–Cummings Model

The Jaynes–Cummings model describes a two-level atom interacting with a quantized mode of a cavity in the "good-cavity" limit. The "good-cavity" limit is when the cavity linewidth κ is much smaller than the collective atom-cavity coupling $\sqrt{N}g$ (i.e., $\sqrt{N}g \gg \kappa$). We start with the free evolution Hamiltonian for a two-level atom and a single mode field

$$\hat{H}_0 = \hat{H}_A + \hat{H}_F = \hbar\omega_a \left|e\right\rangle \left\langle e\right| + \hbar\omega_c\Big(\hat{c}^\dagger\hat{c} + \frac{1}{2}\Big), \tag{2.56}$$

where ω_a is the atomic transition frequency and ω_c is the cavity resonance frequency of the field mode. The atom-field interaction Hamiltonian is a modified version of Eq. (2.4), except now we use Eq. (2.52) for the quantized field without $\sin(kz)$ because we assume homogeneous atom-cavity coupling. The atom-field interaction Hamiltonian is then

$$\hat{H}_{AF} = \hbar g(\hat{\sigma} + \hat{\sigma}^\dagger)(\hat{c} + \hat{c}^\dagger). \tag{2.57}$$

In the rotating-wave approximation, we drop the nonconserving energy terms, so Eq (2.57) becomes

$$\hat{H}_{AF} = \hbar g(\hat{c}^\dagger\hat{\sigma} + \hat{c}\hat{\sigma}^\dagger), \tag{2.58}$$

where the atom-cavity coupling constant g is defined as

$$g = -\hat{\varepsilon}\left\langle g\right| \hat{d} \left|e\right\rangle \sqrt{\frac{\omega}{2\hbar\varepsilon_0 V}}. \tag{2.59}$$

The Jaynes–Cummings Hamiltonian while ignoring the vacuum-field energy is

$$\hat{H}_{JC} = \hat{H}_A + \hat{H}_F + \hat{H}_{AF} = \hbar\omega_a \left|e\right\rangle \left\langle e\right| + \hbar\omega_c\hat{c}^\dagger\hat{c} + \hbar g(\hat{c}^\dagger\hat{\sigma} + \hat{c}\hat{\sigma}^\dagger). \tag{2.60}$$

2.3 Analytical and Numerical Methods

In this section, I discuss an analytical and numerical method that allows for larger atom numbers to be simulated, while reducing simulation times. For a more thorough explanation of cumulants I direct the reader to [40] and for Liouville space [26].

2.3.1 Cumulants

As the atom number N increases in our simulations, the scaling of the density matrix $\hat{\rho}$ makes an exact numerical solution of the master equation Eq. (2.36) quickly intractable. The Monte Carlo wave function method [57, 54] can be used to reach higher atom numbers, but the state vector used here soon becomes intractable as well. This is because, as N increases, both the total atomic Hilbert space and the maximum required truncated Fock space used in our simulations increase rapidly. To simulate higher atom numbers above the experimentally observed lasing threshold in [22], we now turn to the use of cumulant theory. Here, the joint cumulant $\langle\cdot\rangle_c$ of n operators is a general measure of correlations between operators. It is given by the generalized culumant expansion method, in which cumulants can be explicitly represented by the lower moments [40]

$$\left\langle \hat{X}_1^{(a_1)} \dots \hat{X}_n^{(a_n)} \right\rangle_c = -\prod_j a_j! \sum_{l=1}^{m} \sum_{\sum_{i=1}^{l} \alpha = a_j} \left(\sum_i k_i - 1 \right)! (-1)^{\sum_i k_i} \prod_{i=1}^{l} \left[\frac{1}{k_i!} \left(\frac{\left\langle \prod_{j=1}^{n} \hat{X}_j^{(b_{ij})} \right\rangle}{\prod_j b_{ij}!} \right)^{k_i} \right], \tag{2.61}$$

where $\hat{X}_i^{(j)}$ represents the operator $\hat{X}_i$ for atom a_j and $\alpha = k_i b_{ij}$. Thus, each term decomposes $m = \sum_{j=1}^{n} a_j$ objects into $\sum_{i=1}^{l} k_i$ subsets, and the total cumulant is a linear combination of products of these subset moments. The first few cumulants can be calculated as [20]

$$\begin{aligned}
\left\langle \hat{X}_i^{(j)} \right\rangle_c &= \left\langle \hat{X}_i^{(j)} \right\rangle, \\
\left\langle \hat{X}_i^{(j)} \hat{X}_k^{(l)} \right\rangle_c &= \left\langle \hat{X}_i^{(j)} \hat{X}_k^{(l)} \right\rangle - \left\langle \hat{X}_i^{(j)} \right\rangle \left\langle \hat{X}_k^{(l)} \right\rangle, \\
\left\langle \hat{X}_i^{(j)} \hat{X}_k^{(l)} \hat{X}_m^{(n)} \right\rangle_c &= \left\langle \hat{X}_i^{(j)} \hat{X}_k^{(l)} \hat{X}_m^{(n)} \right\rangle + 2 \left\langle \hat{X}_i^{(j)} \right\rangle \left\langle \hat{X}_k^{(l)} \right\rangle \left\langle \hat{X}_m^{(n)} \right\rangle \\
&\quad - \left[\left\langle \hat{X}_i^{(j)} \right\rangle \left\langle \hat{X}_k^{(l)} \hat{X}_m^{(n)} \right\rangle + \left\langle \hat{X}_m^{(n)} \right\rangle \left\langle \hat{X}_i^{(j)} \hat{X}_k^{(l)} \right\rangle + \left\langle \hat{X}_k^{(l)} \right\rangle \left\langle \hat{X}_m^{(n)} \hat{X}_i^{(j)} \right\rangle \right].
\end{aligned} \tag{2.62}$$

We now assume that operators are statistically independent of each other, such that $\langle\cdot\rangle_c = 0$ for $n > 1$. We may therefore invert the expressions of Eq. (2.62) in order to derive an expansion of n^{th} order moment in terms of moments on the order of $n-1$ or smaller. For the second and third

order moments we obtain:

$$\begin{aligned}\left\langle \hat{X}_i^{(j)}\hat{X}_k^{(l)}\right\rangle &= \left\langle \hat{X}_i^{(j)}\right\rangle\left\langle \hat{X}_k^{(l)}\right\rangle,\\ \left\langle \hat{X}_i^{(j)}\hat{X}_k^{(l)}\hat{X}_m^{(n)}\right\rangle &= \left\langle \hat{X}_i^{(j)}\right\rangle\left\langle \hat{X}_k^{(l)}\hat{X}_m^{(n)}\right\rangle + \left\langle \hat{X}_m^{(n)}\right\rangle\left\langle \hat{X}_i^{(j)}\hat{X}_k^{(l)}\right\rangle + \left\langle \hat{X}_k^{(l)}\right\rangle\left\langle \hat{X}_m^{(n)}\hat{X}_i^{(j)}\right\rangle\\ &\quad - 2\left\langle \hat{X}_i^{(j)}\right\rangle\left\langle \hat{X}_k^{(l)}\right\rangle\left\langle \hat{X}_m^{(n)}\right\rangle.\end{aligned} \tag{2.63}$$

We focus on the decomposition of second-order moments $\left\langle \hat{X}_i^{(j)}\hat{X}_k^{(l)}\right\rangle = \left\langle \hat{X}_i^{(j)}\right\rangle\left\langle \hat{X}_k^{(l)}\right\rangle$, which corresponds to a mean-field treatment.

2.3.2 Liouville Space

Let us consider an atom with d states, these states are represented as unit vectors of dimension $(d \times 1)$:

$$|x_1\rangle = \begin{pmatrix}1\\0\\\vdots\\0\end{pmatrix},\ |x_2\rangle = \begin{pmatrix}0\\1\\\vdots\\0\end{pmatrix},\ \ldots\ |x_d\rangle = \begin{pmatrix}0\\0\\\vdots\\1\end{pmatrix}, \tag{2.64}$$

and are elements of a d-dimensional Hilbert space, where they form an orthonormal basis. Operators in this Hilbert space are represented as matrices of dimension $(d \times d)$

$$\hat{O} = \begin{pmatrix}O_{11} & \ldots & O_{1d}\\ \vdots & & \vdots\\ O_{d1} & \ldots & O_{dd}\end{pmatrix}. \tag{2.65}$$

In Liouville space the density operator is transformed into a vectorized operator of dimension $(d^2 \times 1)$ and is represented by a superket $||\rangle\rangle$, where the i-th column of the density matrix $\rho_{\bullet 1}$ (counting from the left) is stacked onto the next column.

$$\hat{\rho} = \sum_i \sum_j \rho_{ij}\,|i\rangle \otimes \langle j| \longrightarrow |\hat{\rho}\rangle\rangle = \sum_i \sum_j \rho_{ij}\,|i\rangle \otimes |j\rangle\,, \tag{2.66}$$

$$|\hat{\rho}\rangle\rangle = \begin{pmatrix} \rho_{\bullet 1} \\ \rho_{\bullet 2} \\ \vdots \\ \rho_{\bullet d} \end{pmatrix}, \quad \text{where } \rho_{\bullet i} = \begin{pmatrix} \rho_{1i} \\ \rho_{2i} \\ \vdots \\ \rho_{di} \end{pmatrix}. \tag{2.67}$$

All other operators except for the Liouvillian become $(d^2 \times d^2)$ superoperators by taking the tensor product with the $(d \times d)$ identity operator $\hat{\mathbb{I}}_d$

$$\hat{\mathcal{O}} = \hat{\mathbb{I}}_d \otimes \hat{O}. \tag{2.68}$$

It is important to note that Liouville space is also a Hilbert space, therefore the postulates of quantum mechanics are preserved. In Liouville space we can now simulate the master equation by performing matrix-vector multiplication instead of matrix-matrix multiplication, which greatly reduces our simulation times.

Chapter 3

Mean-Field Floquet Theory for a Three-Level Cold-Atom Laser

3.1 Motivation

Lasing is realized when a pumped medium provides sufficient optical gain for a cavity or resonator mode. This gain is often provided by stimulated emission which needs to overcome the dissipation of cavity photons and the rate of photon reabsorption. Due to the symmetry between stimulated emission and absorption this usually requires population inversion in conventional two-level systems. However, advances in tailoring emission and absorption spectra e.g. by dynamically driving multi-level systems [17] have led to the realization of lasing or amplification without inversion [17, 68, 70, 1, 38, 58, 2], exciton-polariton condensates [3, 13, 67, 7], and photon Bose–Einstein condensates [36, 37].

One main application of lasers relies on their ability to produce coherent and stable light that can be used to probe materials in spectroscopy [27], but also as ultra-stable oscillators in metrology [10, 45]. Often these oscillators are stabilized by using highly engineered cavities that trap the light and shield the coherence against environmental noise [76]. Instead, only recently, it was pointed out that ultra-coherent light can also be extracted directly from atoms with metastable states that possess ultra-narrow linewidths [51]. In this case one requires sufficient control over the atomic external degrees of freedom such that they are trapped or confined within the cavity and sufficiently cooled. One example of such cold-atom lasers is the superradiant laser [51, 4, 59, 12, 42, 66] which uses population inversion on a ultra-narrow transition to achieve lasing in the optical domain with a potential mHz linewidth. However, so far the continuous-wave operation regime of

this laser is elusive because of radiative heating due to the driving and trapping lasers and the need of finding efficient repump schemes. This is why guided atomic beams [8] are currently explored as a potential alternative [72, 9, 18, 44, 33].

Another solution to this problem is the realization of a hybrid device which achieves lasing and, at the same time, cooling and trapping of the atoms [65, 75, 34, 31, 32]. The experiment described in Ref. [22] is a potential platform for such a device where lasing on a narrow line has been realized while a magneto-optical-trap cools and traps the atoms. Moreover, in this setup lasing is achieved without obvious population inversion on the narrow transition, instead the emission spectrum is modified due to a two-photon Raman resonance of a cavity mode and the trapping lasers. Remarkably, one can then achieve lasing by applying a coherent drive to the narrow transition which obtains sufficient population in the excited state without inversion. The theoretical description of such system is challenging because it requires the correct description of the internal and external degrees of the atoms and the cavity field.

In this thesis, as a first step towards such a description, we will provide a simple mean-field approach which allows us to determine the lasing threshold, intensity, and emission frequency. While we do not describe atomic motion in this thesis, we want this theory to be a first benchmark for future theories that describe atomic motion, internal, and cavity degrees of freedom on equal footing. We develop general methods to predict the lasing threshold and emission frequency. Moreover we use a Floquet method to predict the lasing intensity and frequency at steady-state and compare these results to previously used second-order cumulant approaches [32, 62]. Furthermore we highlight the non-linear aspect of this system by showing the existence of bistable lasing and non-lasing solutions, which was also evident in the experiment [23].

This chapter is organized as follows. We begin in Sec. 3.2 by introducing a fully quantum description of the system and then applying the c-number and mean-field approximations. We then analyze the onset of lasing in Sec. 3.3. Here, we preform a stability analysis on a non-lasing state against field fluctuations in Sec. 3.3.1 in order to derive an apparent lasing threshold. We then, in Sec. 3.3.2, introduce a Floquet method to study the lasing intensity and frequency. In Sec. 3.3.3, we

also study the bistability in this setup by analyzing a hysteresis behavior. In Sec. 3.4.1 we compare our mean-field results to a second-order cumulant approximation and we conclude the thesis in Sec. 3.4.2.

3.2 Theoretical Model

3.2.1 System Dynamics

Our theoretical model basically follows the setup and level scheme that has been used in the experiment of Ref. [22], depicted in Fig. 3.1(a), and explained as follows. A cloud of N non-interacting three level atoms composed of two excited states $|e\rangle$ and $|a\rangle$ and one ground state $|g\rangle$, creating a V-level structure [see Fig. 3.1(b)], are cooled and trapped in an optical cavity. We consider the scenario where two external lasers drive the atoms homogeneously. The $|g\rangle \leftrightarrow |a\rangle$ transition with frequency ω_a and lifetime γ_a is driven by an off-resonant laser with Rabi frequency Ω_m and frequency ω_m. The transition $|g\rangle \leftrightarrow |e\rangle$ with frequency ω_e and lifetime γ_e is driven by a second laser with Rabi frequency Ω_p and frequency ω_p. In addition, the $|g\rangle \leftrightarrow |e\rangle$ also couples to a cavity mode with resonance frequency ω_c, linewidth κ, and a vacuum coupling g_c. The dynamics of the system is described by a Born–Markov master equation. This describes the time evolution of the density operator of both the atomic and cavity degrees of freedom $\hat{\rho}_{AF}$ and takes the form

$$\partial_t \hat{\rho}_{AF} = \frac{1}{i\hbar}\left[\hat{H}, \hat{\rho}_{AF}\right] + \hat{\mathcal{L}}_d \hat{\rho}_{AF}, \tag{3.1}$$

where we have used $\partial_t = \partial/(\partial t)$. The coherent dynamics of the atom-cavity system is given by the Hamiltonian

$$\begin{aligned}\hat{H} = \hbar\Delta_c'\hat{c}^\dagger\hat{c} + \sum_{j=1}^{N}\Big\{ &-\hbar\Delta_p\hat{\sigma}_{ee}^{(j)} - \hbar\Delta_m\hat{\sigma}_{aa}^{(j)} + \frac{\hbar\Omega_p}{2}\left(\hat{\sigma}_{ge}^{(j)} + \hat{\sigma}_{eg}^{(j)}\right) + \frac{\hbar\Omega_m}{2}\left(\hat{\sigma}_{ga}^{(j)} + \hat{\sigma}_{ag}^{(j)}\right) \\ &+ \hbar g_c\left(\hat{c}^\dagger\,\hat{\sigma}_{ge}^{(j)} + \hat{c}\hat{\sigma}_{eg}^{(j)}\right)\Big\},\end{aligned} \tag{3.2}$$

where $\hat{c}$ ($\hat{c}^\dagger$) is the annihilation (creation) operator of the cavity mode and $\hat{\sigma}_{kl}^{(j)} = |k\rangle_j \langle l|_j$ is the transition matrix element of an atom indexed by j between the states $k, l \in \{g, e, a\}$. The Hamiltonian is reported in the frame where the cavity and $|e\rangle$ state rotates with frequency ω_p

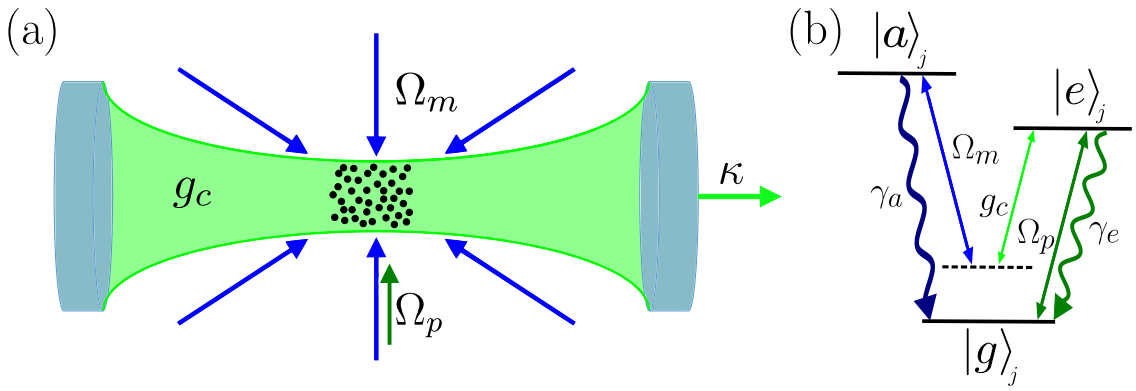

Figure 3.1: (a) Sketch of an ensemble of N three-level atoms coupling to a high-finesse optical cavity and driven by two external lasers. (b) V-shaped atomic level diagram of atom j. The $|g\rangle \leftrightarrow |e\rangle$ transition is driven by the coherent pump laser and is coupled to the cavity mode while the $|g\rangle \leftrightarrow |a\rangle$ transition is driven by a MOT laser.

and the $|a\rangle$ state rotates with frequency ω_m. In this rotating frame we introduce the detunings $\Delta_c' = \Delta_c - \Delta_p$, $\Delta_c = \omega_c - \omega_e$, $\Delta_p = \omega_p - \omega_e$, and $\Delta_m = \omega_m - \omega_a$. The dissipative dynamics of the atom-cavity system are encapsulated by the Lindblad superoperator $\mathcal{L}_d$ given by

$$\hat{\mathcal{L}}_d = \kappa \hat{\mathcal{D}}\left[\hat{c}\right] + \sum_{j=1}^{N} \left\{ \gamma_e \hat{\mathcal{D}}\left[\hat{\sigma}_{ge}^{(j)}\right] + \gamma_a \hat{\mathcal{D}}\left[\hat{\sigma}_{ga}^{(j)}\right] \right\}, \tag{3.3}$$

with $\hat{\mathcal{D}}\left[\hat{J}\right]\hat{\rho}_{AF} = \hat{J}\hat{\rho}_{AF}\hat{J}^\dagger - \left(\hat{J}^\dagger\hat{J}\hat{\rho}_{AF} + \hat{\rho}_{AF}\hat{J}^\dagger\hat{J}\right)/2$ for a jump operator $\hat{J}$.

3.2.2 Parameter Regime and Lasing Mechanism

Following the experimental setup of Ref. [22], we consider the parameters associated with the states $|g\rangle \equiv {}^1S_0$, $|e\rangle \equiv {}^3P_1$, and $|a\rangle \equiv {}^1P_1$ in ^{174}Yb. We mention here that similar parameter regimes can also be realized with other elements such as ^{40}Ca and ^{88}Sr. Here, the $|g\rangle \leftrightarrow |a\rangle$ transition is dipole-allowed resulting in a much broader linewidth compared to the narrow dipole-forbidden $|g\rangle \leftrightarrow |e\rangle$ transition (i.e., $\gamma_e \ll \gamma_a$). In Ref. [22], the laser that is driving the $|g\rangle \leftrightarrow |a\rangle$ transition is also used to cool and trap the atoms in a magneto-optical trap (MOT) which is why we denote this driving laser as the MOT laser (see also the subscript m in $\Omega_m, \omega_m, \Delta_m$) and is red-detuned from resonance $\Delta_m < 0$. A second laser denoted as the pump laser (see also the subscript p in $\Omega_p, \omega_p, \Delta_p$) drives the $|g\rangle \leftrightarrow |e\rangle$ transition. This will usually be operated close to resonance $\Delta_p \approx 0$ with a high power $\Omega_p \gg \gamma_e$ such that sufficiently many atoms can be pumped into the $|e\rangle$ state and undergo the resonant Raman transition. The cavity resonance is chosen such that the decay from $|e\rangle$ to $|g\rangle$ via emitting a cavity photon is far-off resonant, $|\Delta_c'| \gg \kappa, \gamma_e$.

However, the two-photon transition, $|e\rangle$ to $|g\rangle$ by emitting a cavity photon and then $|g\rangle$ to $|a\rangle$ by absorbing a photon from the MOT laser is resonant, $\Delta_c' \approx \Delta_m$ [see Fig. 3.1(b)]. This process allows the $|e\rangle$ state to decay back to $|g\rangle$ via emitting a cavity photon, absorbing a MOT laser photon and then subsequent spontaneous emission inducing a transition from $|a\rangle$ to $|g\rangle$. This rate, for $\Delta_c' \approx \Delta_m$, can be estimated as $\gamma_{\text{eff}} \approx g^2\Omega_m^2/(\gamma_a\Delta_c^2)$. It provides an additional broadening on the $|e\rangle \leftrightarrow |g\rangle$ transition which one can usually neglect at the single-particle level $\gamma_{\text{eff}} \ll \gamma_e$. However, it provides a gain G for emission into the cavity mode which is proportional to the number of atoms

in the $|e\rangle$ state times γ_{eff}, thus $G = N\gamma_{\text{eff}} \langle\hat{\sigma}_{ee}\rangle$.

Lasing is realized in this model if this gain exceeds the losses L of the cavity given by $L = \kappa$, which leads to a qualitative inequality to achieve lasing $\hat{c}$. While this inequality is oversimplified, since it excludes various light-shifts and additional broadening effects, it captures the main idea behind the lasing mechanism, that is the balance of gain and losses. We emphasize there is no population inversion needed between the states $|e\rangle$ and $|g\rangle$, instead one simply requires enough atoms in the $|e\rangle$ state such that the mean number of atoms in the $|e\rangle$ state satisfies $\langle\hat{\sigma}_{ee}\rangle > \kappa/(N\gamma_{\text{eff}})$. A central purpose of this work is to develop a simple theoretical model that can predict the laser threshold and intensity while including the appearing light shifts and broadening mechanisms that are introduced by the two driving lasers. Such a description is needed because the simplified picture given above does completely ignore that $|g\rangle \leftrightarrow |e\rangle$ and $\hat{c}$ must have various frequency components including the frequency of the pump but also the frequency of the laser light in the cavity. To provide such a description we use a mean-field method that we introduce in the next section.

3.2.3 Mean-Field Theory

While the master equation Eq. (3.1) fully encapsulates the dynamics we wish to evaluate, it is not convenient to use for numerical simulations other than for extremely small atom numbers $N \sim \mathcal{O}(1)$. This is not only because the atomic Liouville space scales as 9^N, but also because the cavity field in the lasing regime is assumed to be extremely large $\langle\hat{c}^\dagger\hat{c}\rangle \gg 1$ and therefore requires a substantial number of Fock states to model quantum mechanically.

To overcome this obstacle, we now invoke approximative methods. The first approximation is a mean-field approximation. Here, we assume the atomic density operator is achieved by tracing over the cavity degrees of freedom $\hat{\rho}_A = \text{Tr}_\text{F}(\hat{\rho}_{AF})$ factorizes into mean-field density matrices $\hat{\rho}_j$ such that $\hat{\rho}_A = \bigotimes_j \hat{\rho}_j$, where the tensor product runs over all particles indexed by j. In addition, we assume that all of these density operators are identical, $\hat{\rho} = \hat{\rho}_j$, which is motivated by the permutation symmetry of the master equation Eq. (3.1). To be able to simulate the cavity field, we assume it is always in a coherent field $\hat{\rho}_F = \text{Tr}_\text{A}(\hat{\rho}_{AF}) = |\alpha\rangle\langle\alpha|$, when we partially trace out the

atoms. In this simplified assumption, we completely throw away fluctuations in the field. Instead of evolving the cavity degrees of freedom, we simply simulate the complex field α, by the following equation $\partial_t \alpha = \mathrm{Tr_F}(\hat{c}\partial_t|\alpha\rangle\langle\alpha|)$, which results in

$$\partial_t \alpha = -\left(i\Delta_c' + \frac{\kappa}{2}\right)\alpha - iNg_c\left\langle\hat{\sigma}_{ge}^{(1)}\right\rangle, \tag{3.4}$$

where $\left\langle\hat{\sigma}_{ge}^{(1)}\right\rangle = \mathrm{Tr}\left(\hat{\sigma}_{ge}^{(1)}\hat{\rho}_1\right)$. The evolution of $\hat{\rho}_1$ can now be derived using Eq. (3.1) and tracing out the cavity degrees of freedom and all atoms except for one. This results in the mean-field master equation

$$\partial_t \hat{\rho}_1 = \hat{\mathcal{L}}_A\hat{\rho}_1 + \hat{\mathcal{L}}_F[\alpha]\hat{\rho}_1. \tag{3.5}$$

Here, the atomic Liouvillian superoperator is given by

$$\hat{\mathcal{L}}_A\hat{\rho}_1 = \frac{1}{i\hbar}\left[\hat{H}_A, \hat{\rho}_1\right] + \left(\gamma_e\hat{\mathcal{D}}\left[\hat{\sigma}_{ge}^{(1)}\right] + \gamma_a\hat{\mathcal{D}}\left[\hat{\sigma}_{ga}^{(1)}\right]\right)\hat{\rho}_1, \tag{3.6}$$

with the atomic Hamiltonian defined as

$$\hat{H}_A = -\hbar\Delta_p\hat{\sigma}_{ee}^{(1)} - \hbar\Delta_m\hat{\sigma}_{aa}^{(1)} + \frac{\hbar\Omega_p}{2}\left(\hat{\sigma}_{ge}^{(1)} + \hat{\sigma}_{eg}^{(1)}\right) + \frac{\hbar\Omega_m}{2}\left(\hat{\sigma}_{ga}^{(1)} + \hat{\sigma}_{ag}^{(1)}\right), \tag{3.7}$$

while the Liouvillian describing the coupling with the coherent field becomes

$$\hat{\mathcal{L}}_F\left[\alpha\right]\hat{\rho}_1 = \frac{1}{i\hbar}\left[\hat{H}_F\left(\alpha\right), \hat{\rho}_1\right], \tag{3.8}$$

with the field Hamiltonian given by

$$\hat{H}_F\left(\alpha\right) = \hbar g_c\left(\alpha^*\hat{\sigma}_{ge}^{(1)} + \alpha\hat{\sigma}_{eg}^{(1)}\right). \tag{3.9}$$

The system of coupled differential equations for $\hat{\rho}_1$ and α is at the basis of our theoretical mean-field analysis. We first mention by employing this mean-field analysis, we can now simulate only a single atom that couples to a coherent field which sees N identical atoms. By doing this we have simplified the simulation of the full master equation Eq. (3.1) to the simulation of one complex variable α and a 3×3 density matrix $\hat{\rho}_1$. As a consequence, however, we have found a non-linear term $\hat{\mathcal{L}}_F\left[\alpha\right]$, which introduces a mean-field coupling between the atoms mediated by the cavity field.

3.3 Lasing Analysis

Having established the setup and a simple mean-field model of the system, we now study the lasing regime. We do this using two different analytical methods that reveal the lasing threshold, lasing frequency, and field amplitudes in various parameter regimes.

3.3.1 Stability Analysis

To begin, we find a set of solutions to the atom-cavity system, $(\hat{\rho}_0, \alpha_0)$[1] , in the non-lasing regime after it has reached steady-state, $\partial_t \alpha_0 = 0$ and $\partial_t \hat{\rho}_0 = 0$. We solve these equations self-consistently with the result

$$\alpha_0 = \frac{-iNg_c \operatorname{Tr}\left(\hat{\sigma}_{ge}^{(1)} \hat{\rho}_0\right)}{i\Delta_c' + \frac{\kappa}{2}}, \tag{3.10}$$

where we have used Eq. (3.5) to find the steady-state of the atom $\hat{\rho}_0$. The mean-field component α_0 in the non-lasing regime is often considered to be zero. This is not true in our case because the pump laser drives the $|g\rangle \leftrightarrow |e\rangle$ transition and therefore induces a non-vanishing dipole moment $\operatorname{Tr}\left(\hat{\sigma}_{ge}^{(1)} \hat{\rho}_0\right)$. This is the pump laser field that is scattered by the atoms into the cavity and is small due to the choice of our parameters in which Δ_c is a large frequency but not negligible.

In order to find the transition from a non-lasing to a lasing state, we have to analyze fluctuations around the solution $(\hat{\rho}_0, \alpha_0)$. Those fluctuations are denoted by $\delta\alpha = \alpha - \alpha_0$ and $\delta\hat{\rho} = \hat{\rho}_1 - \hat{\rho}_0$ and are physically always present, e.g. due to external noise but also due to quantum fluctuations. The linearized equations of motion for the fluctuations are given by

$$\partial_t \delta\hat{\rho} = \left(\hat{\mathcal{L}}_A + \hat{\mathcal{L}}_F[\alpha_0]\right) \delta\hat{\rho} + \hat{\mathcal{L}}_F[\delta\alpha]\hat{\rho}_0, \tag{3.11}$$

and

$$\partial_t \delta\alpha = -\left(i\Delta_c' + \frac{\kappa}{2}\right) \delta\alpha - iNg_c \operatorname{Tr}\left(\hat{\sigma}_{ge}^{(1)} \delta\hat{\rho}\right), \tag{3.12}$$

where we have neglected terms that are second-order in fluctuations and used the steady-state

[1] Variables with subscript 0 are in steady-state.

relation in Eq. (3.10). We now use the Laplace transformation,

$$L[f(t)](s) = \int_0^\infty f(t)e^{-st}\,dt, \tag{3.13}$$

to find the linear and coupled equations of $L[\delta\alpha]$, $L[\delta\hat{\rho}]$, and $L[\delta\alpha^*]$. After eliminating $L[\delta\hat{\rho}]$ from those equations, we get two linearly coupled equations for $L[\delta\alpha]$ and $L[\delta\alpha^*]$ given by

$$\mathbf{C}(s)\vec{\mathbf{b}}(s) = \vec{\mathbf{x}}(s), \tag{3.14}$$

where we have introduced

$$\vec{\mathbf{b}} = \begin{pmatrix} L[\delta\alpha] \\ L[\delta\alpha^*] \end{pmatrix}, \quad \vec{\mathbf{x}} = \begin{pmatrix} \delta\alpha(0) - iNg_cZ(s) \\ \delta\alpha^*(0) + iNg_cZ^*(s) \end{pmatrix}, \tag{3.15}$$

and the 2×2 coupling matrix $\mathbf{C}$ with entries $\mathbf{C}_{ab}$ $[a, b \in \{1, 2\}]$ given by

$$\mathbf{C}_{11}(s) = s + i\Delta_c' + \frac{\kappa}{2} + Ng_c^2Y(s) = \mathbf{C}_{22}^*(s), \tag{3.16}$$

and

$$\mathbf{C}_{12}(s) = Ng_c^2X(s) = \mathbf{C}_{21}^*(s). \tag{3.17}$$

Here, we have used the definitions

$$\begin{aligned} X(s) &= \mathrm{Tr}\Big(\hat{\sigma}_{ge}^{(1)}W^{-1}(s)[\hat{\sigma}_{ge}^{(1)}, \hat{\rho}_0]\Big), \\ Y(s) &= \mathrm{Tr}\Big(\hat{\sigma}_{ge}^{(1)}W^{-1}(s)[\hat{\sigma}_{eg}^{(1)}, \hat{\rho}_0]\Big), \\ Z(s) &= \mathrm{Tr}\Big(\hat{\sigma}_{ge}^{(1)}W^{-1}(s)\delta\hat{\rho}(0)\Big), \end{aligned} \tag{3.18}$$

and

$$W(s) = s - \hat{\mathcal{L}}_A - \hat{\mathcal{L}}_F[\alpha_0]. \tag{3.19}$$

Details of this derivation have been shifted to Appendix A. Equation (3.14) can now be solved by inverting $\mathbf{C}(s)$ for every value of s.

The stability of the non-lasing solution $(\hat{\rho}_0, \alpha_0)$ is determined by whether $\delta\alpha(t)$ is exponentially damping (stable) or exponentially growing (unstable). Stability for the fields thus require that all poles s_n of the Laplace transformed fields $\vec{\mathbf{b}}(s)$ have a negative real part. This is true since

such a pole s_n results in a field $\delta\alpha \propto e^{s_n t}$. To determine the stability, it is then sufficient to find the primary solution s_0 with the largest real component. Before finding s_0, we first mention that an instability cannot occur from a pole of $Z(s)$. This is true since all values of s for which W Eq. (3.19) is not invertible are negative which is equivalent to the statement that the spectrum of $\hat{\mathcal{L}}_A + \hat{\mathcal{L}}_F[\alpha_0]$ consists of numbers with negative real part. Then, the only way to find an instability is by a pole coming from inverting $\mathbf{C}(s)$. These poles can be found as the roots of the determinant of $\mathbf{C}(s)$ which is called the dispersion relation

$$D(s) = \det\left[\mathbf{C}(s)\right]. \tag{3.20}$$

Using this result, we can now numerically find s_0 by calculating the zero with the largest real part of Eq. (3.20). We plot the real and imaginary parts of this primary root in Fig. 3.2. The special case of when $\mathrm{Re}\,(s_0) = 0$ is the threshold value of the lasing transition, which we calculate numerically and display as a red dashed line in Fig. 3.2. When $\mathrm{Re}\,(s_0) < 0$, the non-lasing solution is stable and $\mathrm{Re}\,(s_0)$ determines the decay rate of the fluctuations. Meanwhile, the imaginary part $\mathrm{Im}\,(s_0)$ determines the frequency of the light emission as $\delta\alpha \propto \exp(i\,\mathrm{Im}\,(s_0)\,t)$. If $\mathrm{Re}\,(s_0) > 0$, we expect an exponential increase in the field fluctuations, indicating that the initial state of a non-lasing solution was unstable. Dynamically we would expect that this results on longer timescales in a large cavity light field or lasing.

It might be interesting to compare the mean-field results in Fig. 3.2 with our simplified threshold $\langle\hat{\sigma}_{ee}\rangle = \kappa/(N\gamma_{\mathrm{eff}}) \approx 3\times10^3/N$ that we introduced in Sec. 3.2.2. For large pump power we expect $\langle\hat{\sigma}_{ee}\rangle \approx 0.5$ resulting in a threshold at $N \approx 6000$. This is in fact close to the lower bound of the threshold (red dashed line) visible in Figs. 3.2(a) and (b). The curvature of the red line is likely due to $\langle\hat{\sigma}_{ee}\rangle \approx 0.5$ being violated if the pump laser becomes off-resonant. It might seem surprising that the lowest critical value of N is not found at $\Delta_p = 0$. However, this can be partially explained by the existence of an AC-Stark shift that is induced by the MOT laser. Since the MOT laser is red detuned from the $|g\rangle \leftrightarrow |a\rangle$ transition, it shifts the resonance of the $|g\rangle$

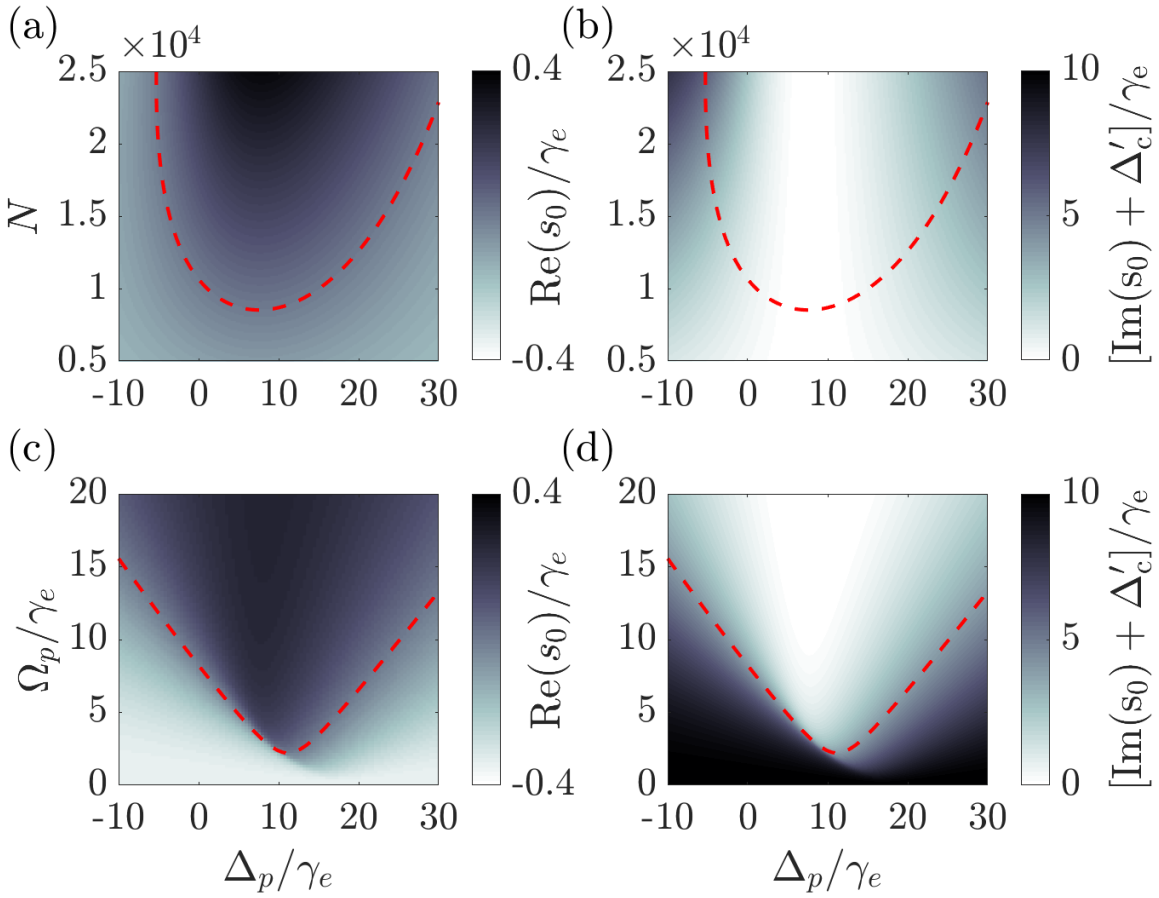

Figure 3.2: (a) The real component $\mathrm{Re}(s_0)$ and (b) imaginary component $\mathrm{Im}(s_0)$ of the primary zero s_0, which possesses the largest real component of $D(s)$ in Eq. (3.20), as a function of the pump detuning and atom number. (c)–(d) The real and imaginary part of the zero s_0, respectively, as a function of the pump Rabi frequency and the pump detuning Δ_p. The red dashed line is the lasing threshold in which $\mathrm{Re}(s_0) = 0$. The common parameters for all plots are $\Delta_c = -192\gamma_e$, $\Delta_m = -192\gamma_e$, $g_c = 0.33\gamma_e$, $\gamma_a = 159\gamma_e$, $\Omega_m = \gamma_a/2$, and $\kappa = 0.39\gamma_e$. Meanwhile, (a)–(b) has $\Omega_p = \sqrt{140}\gamma_e$ and (c)–(d) has $N = 20000$.

transition relative to the $|e\rangle$ transition down by an amount of

$$\Delta_{AC,MOT} \approx -\frac{\Omega_m^2}{4\Delta_m}, \tag{3.21}$$

which is $\Delta_{AC,MOT} \approx 8.23\gamma_e$ for our parameters. We can then compensate this shift by using a blue detuned pump laser.

A similar shift is also found in Figs. 3.2(c) and (d). Here, the threshold line seems to be nearly symmetric with respect to its minimum. Such a behavior is expected, according to our considerations in Sec. 3.2.2. In fact the critical pump power in this picture is solely meant to pump enough atoms in the $|e\rangle$ state. The population of this state approaches 0.5 for a diverging value of $\Omega_p^2/\big((\Delta_p - \Delta_p^{\mathrm{opt}})^2 + \Gamma^2/4\big)$. Here Γ is the effective linewidth of $|e\rangle$ and Δ_p^{opt} accounts for all frequency shifts. Thus we would expect the critical value of Ω_p to scale with $\sqrt{(\Delta_p - \Delta_p^{\mathrm{opt}})^2 + \Gamma^2}$, which is symmetric in Δ_p around Δ_p^{opt} and also explains the linear slope of the red line in Figs. 3.2(c) and (d) for large detuning $|\Delta_p|$. The asymmetry of the transition line in Figs. 3.2(a) and (b) is likely due to a dependence of Δ_p^{opt} and Γ on N.

Finally we want to discuss the results of $\mathrm{Im}(s_0)$ that are visible in false colors in Figs. 3.2(b) and (d). We find that close to the lasing threshold the frequency of the amplified light field is $\mathrm{Im}(s_0) \approx -\Delta_c'$. This means that, since all equations are reported in a reference frame where $\hat{a}$ rotates with $-\omega_p$, the light is emitted approximately in resonance with ω_c. Nevertheless, we find a non-negligible shift of the light emitted into the cavity, which can be far detuned from the cavity resonance with respect to the cavity linewidth, especially for the case of a off-resonant pump laser.

3.3.2 Floquet Method

While the stability analysis offers insight about the onset of the lasing dynamics, it inherently assumes an underlying non-lasing solution. This stability analysis can be used to calculate the lasing threshold. However, it cannot be used to calculate the intensity and frequency at steady state of the actual lasing solution.

To find a description for the lasing solution, we now employ a Floquet method. We assume the field and atomic density operator can be decomposed in components corresponding to multiples of the frequency ω. The frequency ω has to be found self-consistently. We first make a Fourier decomposition of the field and atomic density operator into $2m+1$ components for some cutoff frequency $\omega_{\text{cut}} = m\omega$. The decomposition of α and $\hat{\rho}$ is a sum of time-independent amplitudes given by

$$\alpha = \sum_{n=-m}^{m} \alpha_n e^{i\omega n t}, \quad \hat{\rho} = \sum_{n=-m}^{m} \hat{\rho}_n e^{i\omega n t}. \tag{3.22}$$

Substituting this into Eqs. (3.11) and (3.12) results in

$$i\omega n \hat{\rho}_n = \hat{\mathcal{L}}_A \hat{\rho}_n + \sum_{n'=-m}^{m} \left(\hat{\mathcal{G}}_u[\alpha_{n-n'}] + \hat{\mathcal{G}}_d[\alpha^*_{n'-n}] \right) \hat{\rho}_{n'}, \tag{3.23}$$

and

$$i\omega n \alpha_n = -\left(i\Delta_c' + \frac{\kappa}{2} \right) \alpha_n - iNg_c \operatorname{Tr}(\hat{\sigma}_{ge}\hat{\rho}_n), \tag{3.24}$$

where we introduced $\hat{\mathcal{G}}_u[\alpha]\hat{\rho} = -ig_c\alpha[\hat{\sigma}_{eg}, \hat{\rho}]$ and $\hat{\mathcal{G}}_d[\alpha^*]\hat{\rho} = -ig_c\alpha^*[\hat{\sigma}_{ge}, \hat{\rho}]$, such that we decompose the coupling of the atomic density operator with the field as $\hat{\mathcal{L}}_F[\alpha] = \hat{\mathcal{G}}_u[\alpha] + \hat{\mathcal{G}}_d[\alpha^*]$.

The non-lasing solution, whose stability we have analyzed in the previous Sec. 3.3.1, can be understood as a limiting case of Eq. (3.24) where we impose $\hat{\rho}_n = \alpha_m = 0$ for $m \neq 0$. This is the case when there is, to good approximation, no additional field in the cavity except for the scattered laser light given by α_0 Eq. (3.10). Since this non-lasing solution becomes unstable we expect to observe a component in the sideband α_1, where the frequency ω is close to $-\Delta_c'$. This is by far the largest component and all other components are suppressed due to the cavity linewidth being much smaller than the emission frequency $\kappa \ll \omega$.

Consequently, to a good approximation we can only consider three frequency components which is equivalent to performing a cut-off at $m = 1$. Imposing this cutoff onto Eq. (3.24) and therefore disregarding higher and lower frequency terms, let us rewrite Eq. (3.24) into $\mathfrak{L}(\vec{\boldsymbol{\alpha}}, \omega)\vec{\boldsymbol{\rho}} = \vec{\mathbf{0}}$,

where $\vec{\boldsymbol{\rho}} = (\hat{\rho}_{-1}, \hat{\rho}_0, \hat{\rho}_1)^T$, $\vec{\boldsymbol{\alpha}} = (\alpha_{-1}, \alpha_0, \alpha_1)^T$, and

$$\mathfrak{L}(\vec{\boldsymbol{\alpha}}, \omega) = \begin{pmatrix} -i\omega - \hat{\mathfrak{L}}_0 & -\hat{\mathfrak{L}}_{-1} & 0 \\ -\hat{\mathfrak{L}}_1 & -\hat{\mathfrak{L}}_0 & -\hat{\mathfrak{L}}_{-1} \\ 0 & -\hat{\mathfrak{L}}_1 & i\omega - \hat{\mathfrak{L}}_0 \end{pmatrix}. \tag{3.25}$$

The elements of $\mathfrak{L}(\vec{\boldsymbol{\alpha}}, \omega)$ are given by

$$\hat{\mathfrak{L}}_{-1} = \hat{\mathcal{G}}_u[\alpha_{-1}] + \hat{\mathcal{G}}_d[\alpha_1^*], \tag{3.26}$$

$$\hat{\mathfrak{L}}_0 = \hat{\mathcal{L}}_A + \hat{\mathcal{G}}_u[\alpha_0] + \hat{\mathcal{G}}_d[\alpha_0^*], \tag{3.27}$$

and

$$\hat{\mathfrak{L}}_1 = \hat{\mathcal{G}}_u[\alpha_1] + \hat{\mathcal{G}}_d[\alpha_{-1}^*]. \tag{3.28}$$

We can now find the steady-state $\vec{\boldsymbol{\rho}}(\vec{\boldsymbol{\alpha}}, \omega)$ by calculating the kernel of $\mathfrak{L}(\vec{\boldsymbol{\alpha}}, \omega)$ and imposing the normalization condition. This steady-state depends on the choice of the field $\vec{\boldsymbol{\alpha}}$ and frequency ω which has to be updated self-consistently. To do this we calculate

$$\tilde{\vec{\boldsymbol{\alpha}}}(\vec{\boldsymbol{\alpha}}, \omega) = (\tilde{\alpha}_{-1}(\vec{\boldsymbol{\alpha}}, \omega), \tilde{\alpha}_0(\vec{\boldsymbol{\alpha}}, \omega), \tilde{\alpha}_1(\vec{\boldsymbol{\alpha}}, \omega))^T, \tag{3.29}$$

with

$$\tilde{\alpha}_n(\vec{\boldsymbol{\alpha}}, \omega) = \frac{-iNg_c \mathrm{Tr}(\hat{\sigma}_{ge}\hat{\rho}_n(\vec{\boldsymbol{\alpha}}, \omega))}{i(\Delta_c' + \omega n) + \frac{\kappa}{2}}, \tag{3.30}$$

and where $\hat{\rho}_n(\vec{\boldsymbol{\alpha}}, \omega)$ is the n component of the steady-state vector $\vec{\boldsymbol{\rho}}(\vec{\boldsymbol{\alpha}}, \omega)$. Then we define a function

$$F(\vec{\boldsymbol{\alpha}}, \omega) = \sum_{n=-m}^{m} |\alpha_n - \tilde{\alpha}_n(\vec{\boldsymbol{\alpha}}, \omega)|^2, \tag{3.31}$$

such that $F(\vec{\boldsymbol{\alpha}}, \omega) = 0$ results in the realization of a steady-state for the field $\vec{\boldsymbol{\alpha}}$, the state of the atom $\vec{\boldsymbol{\rho}}$ and the frequency ω. We emphasize that one special case of this steady-state solution is the non-lasing state that is imposing $\hat{\rho}_n = \alpha_m = 0$ for $m \neq 0$. Finding a solution $\vec{\boldsymbol{\alpha}}$ and ω of Eq. (3.31)

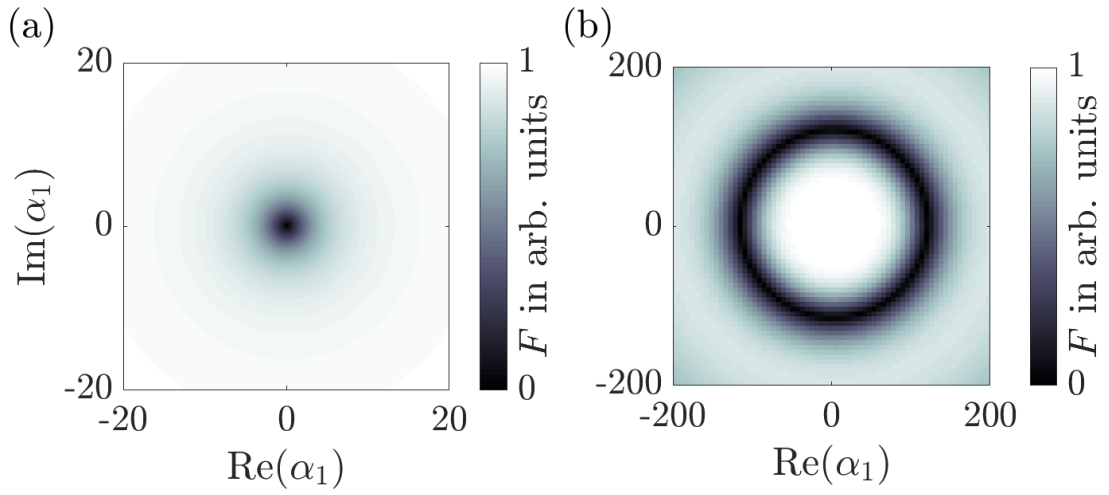

Figure 3.3: (a) The function F defined in Eq. (3.31) in arbitrary units for $N = 20000$, $\Delta_p = 10\gamma_e$, and $\Omega_p = 2\gamma_e$, , $\alpha_0 \approx -3.3 - 2.6i$, $\alpha_1 \approx 0 + 0i$, and $\omega =$ undefined. (b) for $\Omega_p = 15\gamma_e$, $\alpha_0 \approx -5.6 - 1.3i$, $\alpha_1 \approx 0 + 0i$, and $\omega = 205.5\gamma_e$.

is achieved numerically and we show $F(\alpha_{-1}, \alpha_0, \alpha_1, \omega)$ in the non-lasing (a) and lasing regime (b) in Fig. 3.3 for a fixed choice of α_0, α_1 and ω [see caption of Fig. 3.3]. In the non-lasing case we find there is only one zero when $\alpha_{-1} = 0$, as seen Fig. 3.3(a). This indicates that the only light field in the cavity is the scattered laser light by the atoms given by α_0. In the lasing regime Fig. 3.3(b) we find a $U(1)$ symmetric set of solutions indicating a non-vanishing lasing field amplitude $|\alpha_{-1}|^2$ with an arbitrary phase. The found $U(1)$ symmetry is a direct consequence of the underlying equations that are invariant under a transformation

$$\alpha_{-1} \mapsto \alpha_{-1} e^{-i\varphi}, \quad \hat{\rho}_{-1} \mapsto e^{-i\varphi\hat{\sigma}_{ee}} \hat{\rho}_{-1} e^{i\varphi\hat{\sigma}_{ee}}, \tag{3.32}$$

with arbitrary phase φ. This transformation is defined in the Fourier components. Notice that the total field α and atomic density $\hat{\rho}$ is not invariant under this transformation. The appearance of a $U(1)$ symmetric solution is a common feature of laser systems and highlights that the phase of the laser is spontaneously broken. In fact this directly implies that the field α_{-1} is not locked to the phase of an external driving laser.

Using Eq. (3.31) we now find the solution $\vec{\boldsymbol{\alpha}}$ and ω and calculate the total, time-averaged field

$$|\alpha|^2_{\text{av}} = \lim_{t_{\text{av}}\to\infty} \frac{1}{t_{av}} \int_0^{t_{\text{av}}} |\alpha(t)|^2 \, dt = |\alpha_{-1}|^2 + |\alpha_0|^2 + |\alpha_1|^2. \tag{3.33}$$

We are now in a position to reexamine the lasing threshold by studying the intensity of the field for different parameters using our three-component Floquet method. We do this in Fig. 3.4 where we examine the same parameter regimes as in Fig. 3.2 and display the threshold found using the stability analysis as a red dashed line in each plot. The intensities are visible in Fig. 3.4(a) and (c). We find the red dashed line is in good agreement with the onset of a large cavity field for negative and small values of Δ_p. Instead, interestingly, we find there exists a region for large Δ_p in which the stability analysis suggests that the non-lasing solution is stable and yet our Floquet method predicts a large intensity. This implies there exists a bistability, where a lasing and non-lasing solution are both stable.

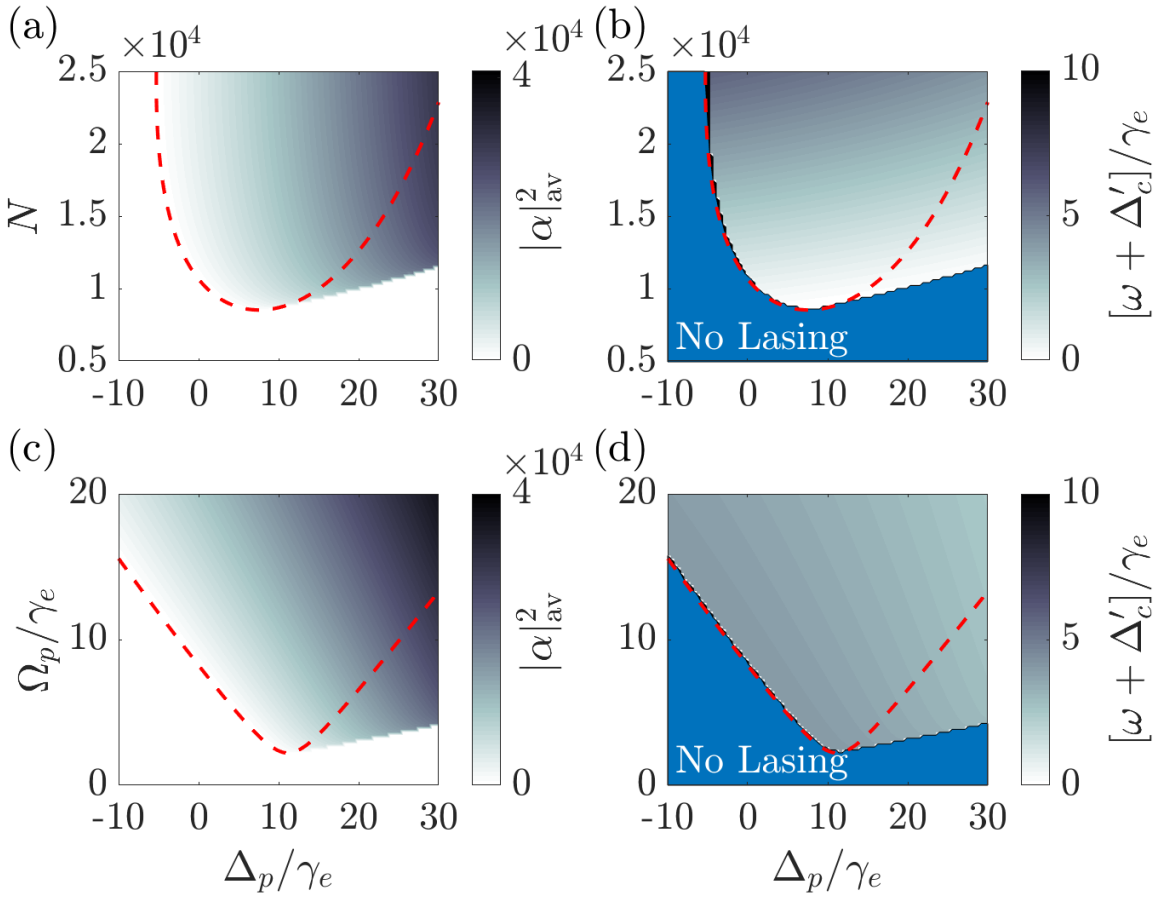

Figure 3.4: Floquet method calculations of the intensity [(a) and (c)] and emission frequency [(b) and (d)] of the lasing field. The first row (a)–(b) shows values as a function of atom number and pump detuning while the second row (c)–(d) plots the values as a function pump Rabi frequency and pump detuning. The red dashed lines were calculated using Eq. (3.20). All parameters are the same as in Fig. 3.2.

In Fig. 3.4(b) and (d) we show the emission frequency ω for the same parameters. In the case where we found $\alpha_{-1} = 0$ this frequency is not defined which we indicate in these plots by the "No Lasing" regime. In the lasing regime we find the frequency ω to be close but detuned from the cavity resonance $-\Delta_c'$. This shows there are non-trivial light-shifts that modify the lasing frequency. As seen in Fig. 3.4(d) this frequency seems to be almost independent of Ω_p and Δ_p, while we see a major dependence of the frequency ω on the atom number N [see Fig. 3.4(d)]. Here, we see an increase of the detuning $\omega + \Delta_c'$ with the number of atoms N.

3.3.3 Hysteresis Regime

Now, we want to study the regime where we expect to have bistable lasing and non-lasing solutions. We do this by dynamically ramping the pump power up and down again. We initialize the system with $\left\langle \hat{\sigma}_{gg}^{(1)}(t=0) \right\rangle = 1$ and $|\alpha(t=0)|^2 \approx 0$, as well as the pump laser being switched off $\Omega_p(t=0) = 0$. This is the non-lasing regime when the cavity field is basically empty. Using this initial state we simulate the dynamics of the field and the mean-field atomic density operator whose evolution is governed by Eq. (3.4) and Eq. (3.5), respectively. While integrating those equations, we sweep the pump Rabi frequency with a linear profile $\Omega_p(t) = At$ with a slow rate A until $\Omega_p = 20\gamma_e$ at time T. This value is chosen such that for all parameters visible in Fig. 3.4 we end up with only the lasing solution. After ramping up the power we ramp the power back down with the same but negative linear slope $-A$ such that $\Omega_p(t) = 20\gamma_e - A(t-T)$ and $\Omega_p(2T) = 0$. We show the ramping scheme as an inset in Fig. 3.5(a).

We perform these simulations for two different detunings representing the parameters where we do not expect to find bistability $\Delta_p = 10\gamma_e$ [see Fig. 3.5(a)] and where we expect to find bistability $\Delta_p = 25\gamma_e$ [see Fig. 3.5(b)]. In Fig. 3.5(a) and (b) we plot the dynamics of the field intensity $|\alpha(t)|^2$ for ramping up the power as gray dotted lines and for ramping down the power as a black solid line. As visible in Fig. 3.5(a) the black line completely overlaps with the gray data point therefore indicating that the lasing solution is the same when ramping up or down the pump power. We also compare the dynamically simulated laser intensity with $|\alpha|^2_{\mathrm{av}}$ obtained from the

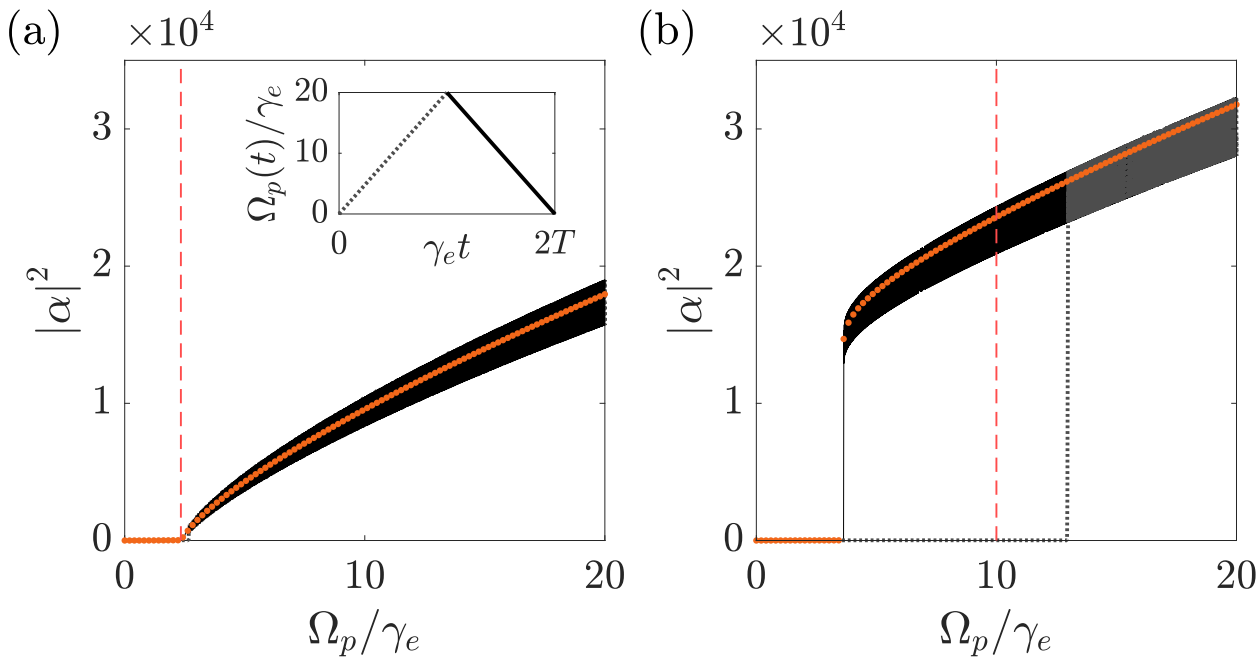

Figure 3.5: Intensity $|\alpha|^2$ as a function of $\Omega_p \propto t$ for 20000 atoms. The evolution uses (a) $\Delta_p = 10\gamma_e$ which should does not possess a hysteresis regime and (b) $\Delta_p = 25\gamma_e$ which has a hysteresis regime for $4\gamma_e \lesssim \Omega_p \lesssim 10\gamma_e$. In both plots, the gray curve represents the "forward" evolution as Ω_p increases linearly, while the black curve represents the "backwards" evolution with Ω_p decreasing linearly, with ramping rate $A \approx 3.1 \times 10^{-4}\gamma_e^2$ and integration time $T = 64000/\gamma_e$. Meanwhile, the red dashed curves are the lasing thresholds calculated from the stability analysis, i.e., when $Re(s_0) = 0$. The orange dotted curves display the value of $|\alpha|^2$ calculated from the Floquet method for a particular pump power. The inset displays the forward and backwards ramping of Ω_p.

mean-field Floquet method displayed as orange dots. We find excellent agreement showing that we adiabatically move along the lasing solution.

In Fig. 3.5(b) we see a different behavior due to the existence of bistability. When ramping up the pump power, the atomic system starts lasing for a pump power that is even beyond the one predicted by the stability analysis (vertical dashed line). We expect this is due to the fact that although our ramp speed A is slow it can never be adiabatic when crossing a transition. When ramping the power down we find that in the regime where we previously found only a very small cavity field, we are now in a lasing regime. The light intensity then suddenly jumps to zero for sufficiently weak pumping $\Omega_p \lesssim 4\gamma_e$. This is in agreement with the mean-field Floquet method (orange dots). Our findings show a clear indication of hysteresis in this atom-cavity system which is highlighting the non-linear nature of the atom-light coupling.

3.4 Discussion and Conclusion

3.4.1 Discussion of the Mean-Field Results

Our analysis treats both atom-atom and atom-cavity interactions at a mean-field level. In addition it is assumed that the field is in a "classical" coherent state which is often a good approximation in laser theory. However, the disregard of fluctuations and correlations only allows us to derive certain properties such as the laser intensity and frequency of the cavity field. In the following we want to benchmark our results with a second-order cumulant approximation which includes fluctuations in the atomic and cavity degrees of freedom to a certain extent.

3.4.2 Second-Order Cumulants vs. Mean-Field Results

The second-order cumulant description is derived by calculating the time derivative of all mean-field values $\langle \hat{A} \rangle$ and second moments $\langle \hat{A}\hat{B} \rangle$ where $\hat{A}, \hat{B}$ are arbitrary single atom operators or the cavity field operator $\hat{c}$. Using permutation symmetry and factorizing third-order moments one can then find a closed set of equations for all first $\langle \hat{A} \rangle$ and second-order moments $\langle \hat{A}\hat{B} \rangle$. The

exact derivation is described in Ref. [61] and also applied to a similar system in Ref. [32]. Since the cumulants also include the dynamics of second moments they are considered to go beyond the mean-field description that is presented in this thesis.

We now want to compare the second-order cumulant approximation with our mean-field results. In a first comparison we analyze the dynamics for parameters above and below the lasing threshold. In Fig. 3.6(a) we show the dynamics of $|\alpha|^2$ calculated from the mean-field results, shown as the black solid line. The dynamics are shown for $\Omega_p = \sqrt{140}\gamma_e$, $\Delta_p = 0$, and $N = 10000$ which is slightly below the lasing transition visible in Fig. 3.2. We compare the dynamics of this mean-field trajectory with the ones of the second-order cumulants results for $|\langle\hat{c}\rangle|^2$ and $\langle\hat{c}^\dagger\hat{c}\rangle$. The mean-field predicts a very similar trajectory compared to $|\langle\hat{c}\rangle|^2$ while $\langle\hat{c}^\dagger\hat{c}\rangle$ is significantly higher. The reason for this is that the mean-field result α is mostly dominated by the coherently scattered laser field [see Eq. (3.10)]. This is also described as a coherent field in the second-order cumulants as $\langle\hat{c}\rangle$. However, the second-order cumulants also describe the incoherent field $\langle\hat{c}^\dagger\hat{c}\rangle - |\langle\hat{c}\rangle|^2$ which is significant below the lasing threshold. Above the lasing threshold for $N = 20000$ and same pump power $\Omega_p = \sqrt{140}\gamma_e$ and detuning $\Delta_p = 0$ we show the dynamics of the mean-field and second-order cumulant description in Fig. 3.6(b). Now we observe that the mean-field trajectory α oscillates around the mean intensity $\langle\hat{c}^\dagger\hat{c}\rangle$ of the second-order cumulant description. The coherent field amplitude $|\langle\hat{c}\rangle|^2$ of the second-order cumulant description is instead very small. Here, the scattered laser field is just a minor part of the total light field which explains the small value of $|\langle\hat{c}\rangle|^2$. Instead the lasing field that oscillates approximately at the cavity resonance is much more intense. This lasing field is described completely differently by the mean-field and the second-order cumulant descriptions. In mean-field this lasing field is purely coherent and achieved by breaking an underlying $U(1)$ symmetry. Our mean-field approach assumes a vanishing linewidth of this lasing field, which is an artifact of our approach coming from ignoring noise. The second-order cumulant description includes noise to a certain extent therefore the lasing field has a finite linewidth. The latter results in the fact that this lasing field is described as a incoherent component. Notice that the lasing component in mean-field $|\alpha_{-1}|^2 \approx \langle\hat{c}^\dagger\hat{c}\rangle - |\langle\hat{c}\rangle|^2$ is approximately the incoherent light field

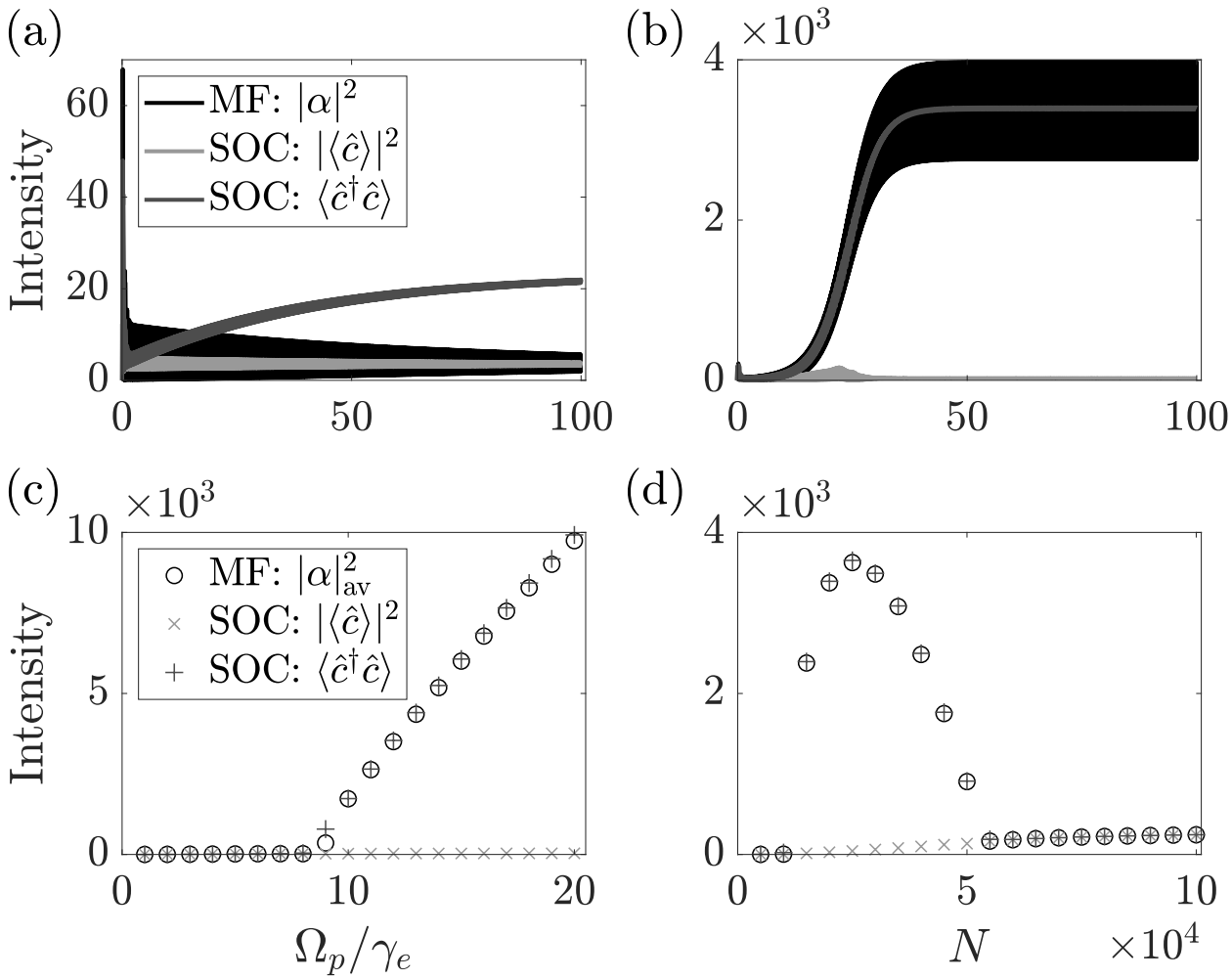

Figure 3.6: Dynamical comparison of the intensity $|\alpha|^2$ for mean-field (MF, black curves) and $\langle\hat{c}^\dagger\hat{c}\rangle$ for second-order cumulants (SOC, dark gray curves). Also shown is the coherent component of the field $|\langle c\rangle|^2$ from the second-order code (light gray curves). The evolution uses the same parameters as Fig. 3.2 expect: (a) $N = 10000$, $\Omega_p = \sqrt{140}\gamma_e$, $\Delta_p = 0$; (b) $N = 20000$, $\Omega_p = \sqrt{140}\gamma_e$, $\Delta_p = 0$; Steady-state intensities of MF (circles), SOC (pluses), and SOC coherent field ($\times$'s) as a function of Ω_p. The parameters are the same as in Fig. 3.2 with $N = 20000$ and $\Delta_p = 0$.

in the second-order cumulant theory. This analysis shows the power and also the limitations of the discussed mean-field theory. Mean-field theory can describe the lasing intensity and dynamics, however, it completely fails to describe the coherence time of this lasing field and instead assumes it is completely coherent.

To compare the second-order cumulant results of the intensity to that of a mean-field description, we show different thresholds as function of Ω_p and N in Fig. 3.6(c) and (d). We find good agreement of the time-averaged mean-field intensity $|\alpha|^2_{\text{av}}$ and the second-order cumulant results for $\langle \hat{c}^\dagger \hat{c} \rangle$ across the non-lasing to lasing transitions. Moreover, we observe that both mean-field and second-order cumulants predict a lasing transition at sufficiently large atom number N and again a transition to non-lasing for even larger atom number N [see Fig. 3.6(d)]. The second transition is explained by a increasing frequency shift for increasing atom number N as it was also noticed in the emission frequency of Fig. 3.4(b). We expect that this shift eventually becomes too large to achieve enough population in $|e\rangle$ state and therefore leads again to a non-lasing configuration. The fact that this is described by both mean-field and second-order cumulant descriptions, is a strong indicator for mean-field being reliable to describe the correct frequency shifts.

3.4.3 Conclusion

In this thesis, we developed a theoretical model to study a lasing scheme of V-level atoms trapped in an optical cavity. Our model employed a mean-field approximation of the cavity field and for the atomic operators which allowed us to simulate the large atom and intracavity photon numbers required to study the lasing transition. We performed a stability analysis of a non-lasing solution which allowed us to find the threshold for lasing and the initial emission frequency. We have analyzed these quantities in terms of changing the pump laser power and frequency as well as the total number of atoms. In addition, we were able to predict the intensity and emission frequency of the lasing solution using a Floquet analysis on the mean-field master equation and cavity field. This Floquet solution shows a $U(1)$ symmetry in one of the frequency components while the total atomic density operator and cavity field does not possess a $U(1)$ symmetry. Furthermore, within

this analysis we were also able to predict a bistable region that we tested by observing a hysteresis within our mean-field approach. Finally we benchmarked our mean-field descriptions with results from a second-order cumulant theory and discussed its validity.

We expect that the methods presented here can be extended in several ways. One possibility is to add noise in the cavity and atomic variables such that we can predict a finite, non-vanishing linewidth of the laser field. In addition it might be interesting to study motion in this model. Motion can result in additional inhomogeneous broadening due to the Doppler shift of emitted photons which might alter the lasing threshold and emission frequency. On the other hand, it might be possible to control the motion of the atom in the lasing regime leading to cooling and trapping in coexistence with lasing [75, 34, 32]. The realization of the latter would be an example of a self-sustainable quantum device which produces coherent light, cools, and traps the atoms at the same time.

Bibliography

[1] G. S. Agarwal, S. Ravi, and J. Cooper. Lasers without inversion: Raman transitions using autoionizing resonances. Phys. Rev. A, 41:4727–4731, May 1990.

[2] Sher Alam. Lasers without inversion and electromagnetically induced transparency. SPIE Optical Engineering Press, 1999.

[3] Pallab Bhattacharya, Bo Xiao, Ayan Das, Sishir Bhowmick, and Junseok Heo. Solid state electrically injected exciton-polariton laser. Phys. Rev. Lett., 110:206403, May 2013.

[4] Justin G. Bohnet, Zilong Chen, Joshua M. Weiner, Dominic Meiser, Murray J. Holland, and James K. Thompson. A steady-state superradiant laser with less than one intracavity photon. Nature, 484(7392):78–81, 2012.

[5] Justin G. Bohnet, Zilong Chen, Joshua M. Weiner, Dominic Meiser, Murray J. Holland, and James K. Thompson. A steady-state superradiant laser with less than one intracavity photon. Nature, 484(7392):78–81, 2012.

[6] Martin M. Boyd. High precision spectroscopy of strontium in an optical lattice: Towards a new standard for frequency and time. January 2007.

[7] Tim Byrnes, Na Young Kim, and Yoshihisa Yamamoto. Exciton-polariton condensates. Nature Physics, 10(11):803–813, Nov 2014.

[8] Chun-Chia Chen, Shayne Bennetts, Rodrigo González Escudero, Benjamin Pasquiou, and Florian Schreck. Continuous guided strontium beam with high phase-space density. Phys. Rev. Applied, 12:044014, Oct 2019.

[9] JingBiao Chen. Active optical clock. Chinese Science Bulletin, 54(3):348–352, Feb 2009.

[10] W. W. Chow, J. Gea-Banacloche, L. M. Pedrotti, V. E. Sanders, W. Schleich, and M. O. Scully. The ring laser gyro. Rev. Mod. Phys., 57:61–104, Jan 1985.

[11] J. I. Cirac. Interaction of a two-level atom with a cavity mode in the bad-cavity limit. Phys. Rev. A, 46:4354–4362, Oct 1992.

[12] Kamanasish Debnath, Yuan Zhang, and Klaus Mølmer. Lasing in the superradiant crossover regime. Phys. Rev. A, 98:063837, Dec 2018.

[13] Hui Deng, Hartmut Haug, and Yoshihisa Yamamoto. Exciton-polariton Bose–Einstein condensation. Rev. Mod. Phys., 82:1489–1537, May 2010.

[14] R. H. Dicke. Coherence in spontaneous radiation processes. Phys. Rev., 93:99–110, Jan 1954.

[15] Albert Einstein. Zur Quantentheorie der Strahlung. Phys. Z., 18:121–128, 1917.

[16] Richard P. Feynman, Frank L. Vernon, and Robert W. Hellwarth. Geometrical representation of the schrödinger equation for solving maser problems. Journal of Applied Physics, 28(1):49–52, 1957.

[17] Michael Fleischhauer, Atac Imamoglu, and Jonathan P. Marangos. Electromagnetically induced transparency: Optics in coherent media. Rev. Mod. Phys., 77:633–673, Jul 2005.

[18] Kazakov G, Dubey S., Famà F., Zhou S., Beli Silva C., Schäffer S.A., Bennetts S., and Schreck F. Towards an active optical clock using an optical conveyor within a ring cavity. In 2021 Joint Conference of the European Frequency and Time Forum and IEEE International Frequency Control Symposium (EFTF/IFCS), pages 1–5, 2021.

[19] Kazakov G, Dubey S., Famà F., Zhou S., Beli Silva C., Schäffer S.A., Bennetts S., and Schreck F. Towards an active optical clock using an optical conveyor within a ring cavity. In 2021 Joint Conference of the European Frequency and Time Forum and IEEE International Frequency Control Symposium (EFTF/IFCS), pages 1–5, 2021.

[20] Crispin W. Gardiner. Handbook of stochastic methods for physics, chemistry and the natural sciences. Springer, 2004.

[21] Christopher Gerry and Peter Knight. Introductory Quantum Optics. Cambridge University Press, 2004.

[22] Hannes Gothe, Dmitriy Sholokhov, Anna Breunig, Martin Steinel, and Jürgen Eschner. Continuous-wave virtual-state lasing from cold ytterbium atoms. Phys. Rev. A, 99:013415, Jan 2019.

[23] Hannes Gothe, Tristan Valenzuela, Matteo Cristiani, and Jürgen Eschner. Optical bistability and nonlinear dynamics by saturation of cold Yb atoms in a cavity. Phys. Rev. A, 99:013849, Jan 2019.

[24] M. Gross and S. Haroche. Superradiance: An essay on the theory of collective spontaneous emission. Physics Reports, 93(5):301 – 396, 1982.

[25] Ivan S. Grudinin and Lute Maleki. Ultralow-threshold Raman lasing with CaF_2 resonators. Opt. Lett., 32(2):166–168, Jan 2007.

[26] Jerryman A Gyamfi. Fundamentals of quantum mechanics in Liouville space. European Journal of Physics, 41(6):063002, oct 2020.

[27] Theodor W. Hänsch. Nobel lecture: Passion for precision. Rev. Mod. Phys., 78:1297–1309, Nov 2006.

[28] L Hilico, C Fabre, and E Giacobino. Operation of a "cold-atom laser" in a magneto-optical trap. Europhysics Letters (EPL), 18(8):685–688, apr 1992.

[29] K. O. Hill, B. S. Kawasaki, and D. C. Johnson. Low-threshold cw raman laser. Applied Physics Letters, 29(3):181–183, 1976.

[30] Tao Hong, Claire Cramer, Eryn Cook, Warren Nagourney, and E. N. Fortson. Observation of the s01–p03 transition in atomic ytterbium for optical clocks and qubit arrays. Opt. Lett., 30(19):2644–2646, Oct ts.

[31] Christoph Hotter, David Plankensteiner, Laurin Ostermann, and Helmut Ritsch. Superradiant cooling, trapping, and lasing of dipole-interacting clock atoms. Opt. Express, 27(22):31193–31206, Oct 2019.

[32] Christoph Hotter, David Plankensteiner, and Helmut Ritsch. Continuous narrowband lasing with coherently driven v-level atoms. New Journal of Physics, 22(11):113021, nov 2020.

[33] Simon B. Jäger, Haonan Liu, John Cooper, Travis L. Nicholson, and Murray J. Holland. Superradiant emission of a thermal atomic beam into an optical cavity. Phys. Rev. A, 104:033711, Sep 2021.

[34] Simon B. Jäger, Minghui Xu, Stefan Schütz, M. J. Holland, and Giovanna Morigi. Semiclassical theory of synchronization-assisted cooling. Phys. Rev. A, 95:063852, Jun 2017.

[35] J.R. Johansson, P.D. Nation, and Franco Nori. Qutip 2: A python framework for the dynamics of open quantum systems. Computer Physics Communications, 184(4):1234 – 1240, 2013.

[36] Peter Kirton and Jonathan Keeling. Nonequilibrium model of photon condensation. Phys. Rev. Lett., 111:100404, Sep 2013.

[37] Jan Klaers, Julian Schmitt, Frank Vewinger, and Martin Weitz. Bose–Einstein condensation of photons in an optical microcavity. Nature, 468(7323):545–548, Nov 2010.

[38] Olga Kocharovskaya. Amplification and lasing without inversion. Physics Reports, 219(3):175–190, 1992.

[39] Sebastian Krämer, David Plankensteiner, Laurin Ostermann, and Helmut Ritsch. Quantumoptics.jl: A Julia framework for simulating open quantum systems. Computer Physics Communications, 227:109 – 116, 2018.

[40] Ryogo Kubo. Generalized cumulant expansion method. Journal of the Physical Society of Japan, 17(7):1100–1120, 1962.

[41] Willis E. Lamb. Theory of an optical maser. Phys. Rev., 134:A1429–A1450, Jun 1964.

[42] Torben Laske, Hannes Winter, and Andreas Hemmerich. Pulse delay time statistics in a superradiant laser with calcium atoms. Phys. Rev. Lett., 123:103601, Sep 2019.

[43] G. Lindblad. On the generators of quantum dynamical semigroups. Communications in Mathematical Physics, 48(2):119–130, 1976.

[44] Haonan Liu, Simon B. Jäger, Xianquan Yu, Steven Touzard, Athreya Shankar, Murray J. Holland, and Travis L. Nicholson. Rugged mhz-linewidth superradiant laser driven by a hot atomic beam. Phys. Rev. Lett., 125:253602, Dec 2020.

[45] Andrew D. Ludlow, Martin M. Boyd, Jun Ye, E. Peik, and P. O. Schmidt. Optical atomic clocks. Rev. Mod. Phys., 87:637–701, Jun 2015.

[46] T. H. Maiman. Stimulated optical radiation in ruby. Nature, 187(4736):493–494, Aug 1960.

[47] Leonard Mandel and Emil Wolf. Optical Coherence and Quantum Optics. Cambridge University Press, 1995.

[48] Krishna K. Meduri, Geoffrey A. Wilson, Peter B. Sellin, and T. W. Mossberg. Dynamically induced irreversibility in coherently driven systems. Phys. Rev. Lett., 71:4311–4314, Dec 1993.

[49] D. Meiser and M. J. Holland. Intensity fluctuations in steady-state superradiance. Phys. Rev. A, 81:063827, Jun 2010.

[50] D. Meiser and M. J. Holland. Steady-state superradiance with alkaline-earth-metal atoms. Phys. Rev. A, 81:033847, Mar 2010.

[51] D. Meiser, Jun Ye, D. R. Carlson, and M. J. Holland. Prospects for a millihertz-linewidth laser. Phys. Rev. Lett., 102:163601, Apr 2009.

[52] D. Meiser, Jun Ye, D. R. Carlson, and M. J. Holland. Prospects for a millihertz-linewidth laser. Phys. Rev. Lett., 102:163601, Apr 2009.

[53] Harold J. Metcalf and Peter van der. Straten. Laser cooling and trapping. Springer, 2002.

[54] Pierre Meystre and Murray Sargent. Elements of Quantum Optics. Springer, 2007.

[55] P.W. Milonni, J.H. Eberly, and E.J.H. coaut. Lasers. A Wiley-Interscience publication. Wiley, 1988.

[56] B. R. Mollow. Stimulated emission and absorption near resonance for driven systems. Phys. Rev. A, 5:2217–2222, May 1972.

[57] Klaus Mølmer, Yvan Castin, and Jean Dalibard. Monte carlo wave-function method in quantum optics. J. Opt. Soc. Am. B, 10(3):524–538, Mar 1993.

[58] J Mompart and R Corbalán. Lasing without inversion. Journal of Optics B: Quantum and Semiclassical Optics, 2(3):R7–R24, may 2000.

[59] Matthew A. Norcia and James K. Thompson. Cold-strontium laser in the superradiant crossover regime. Phys. Rev. X, 6:011025, Mar 2016.

[60] H. M. Pask. Continuous-wave, all-solid-state, intracavity raman laser. Opt. Lett., 30(18):2454–2456, Sep 2005.

[61] David Plankensteiner, Christoph Hotter, and Helmut Ritsch. Quantumcumulants.jl: A Julia framework for generalized mean-field equations in open quantum systems, 2021.

[62] David Plankensteiner, Christoph Hotter, and Helmut Ritsch. QuantumCumulants.jl: A Julia framework for generalized mean-field equations in open quantum systems. Quantum, 6:617, January 2022.

[63] Florentin Reiter and Anders S. Sørensen. Effective operator formalism for open quantum systems. Phys. Rev. A, 85:032111, Mar 2012.

[64] J. J. Sakurai and Jim Napolitano. Modern Quantum Mechanics. Cambridge University Press, 2 edition, 2017.

[65] Thomas Salzburger and Helmut Ritsch. Atomic self-trapping induced by single-atom lasing. Phys. Rev. Lett., 93:063002, Aug 2004.

[66] Stefan A. Schäffer, Mikkel Tang, Martin R. Henriksen, Asbjørn A. Jørgensen, Bjarke T. R. Christensen, and Jan W. Thomsen. Lasing on a narrow transition in a cold thermal strontium ensemble. Phys. Rev. A, 101:013819, Jan 2020.

[67] Christian Schneider, Arash Rahimi-Iman, Na Young Kim, Julian Fischer, Ivan G. Savenko, Matthias Amthor, Matthias Lermer, Adriana Wolf, Lukas Worschech, Vladimir D. Kulakovskii, Ivan A. Shelykh, Martin Kamp, Stephan Reitzenstein, Alfred Forchel, Yoshihisa Yamamoto, and Sven Höfling. An electrically pumped polariton laser. Nature, 497(7449):348–352, May 2013.

[68] Marlan O. Scully and Michael Fleischhauer. Lasers without inversion. Science, 263(5145):337–338, 1994.

[69] Marlan O. Scully and Willis E. Lamb. Quantum theory of an optical maser. i. general theory. Phys. Rev., 159:208–226, Jul 1967.

[70] Marlan O. Scully, Shi-Yao Zhu, and Athanasios Gavrielides. Degenerate quantum-beat laser: Lasing without inversion and inversion without lasing. Phys. Rev. Lett., 62:2813–2816, Jun 1989.

[71] Daniel A. Steck. Quantum and atom optics, 2007.

[72] Vasily V. Temnov. Superradiance and subradiance in the overdamped many-atom micromaser. Phys. Rev. A, 71:053818, May 2005.

[73] D. A. Tieri, Minghui Xu, D. Meiser, J. Cooper, and M. J. Holland. Theory of the crossover from lasing to steady state superradiance, 2017.

[74] Nicholas Werren, Erik Gauger, and Peter Kirton. A quantum model of lasing without inversion, 2022.

[75] Minghui Xu, Simon B. Jäger, S. Schütz, J. Cooper, Giovanna Morigi, and M. J. Holland. Supercooling of atoms in an optical resonator. Phys. Rev. Lett., 116:153002, Apr 2016.

[76] W. Zhang, J. M. Robinson, L. Sonderhouse, E. Oelker, C. Benko, J. L. Hall, T. Legero, D. G. Matei, F. Riehle, U. Sterr, and J. Ye. Ultrastable silicon cavity in a continuously operating closed-cycle cryostat at 4K. Phys. Rev. Lett., 119:243601, Dec 2017.

Appendix A

Laplace Transformation of Field Fluctuations

In this appendix we will show how to calculate the dispersion relation given in Eq. (3.20). Using Eqs. (3.11) and (3.12), the dynamics of $\delta\alpha$ is then governed by

$$\partial_t \delta\alpha = -\left(i\Delta_c' + \frac{\kappa}{2}\right)\delta\alpha - iNg_c \,\mathrm{Tr}(\hat{\sigma}_{ge}\delta\hat{\rho}). \tag{A.1}$$

The Laplace transformation of Eq. (A.1) leads to

$$sL[\delta\alpha] = \delta\alpha(0) - (i\Delta_c' + \frac{\kappa}{2})L[\delta\alpha] - iNg_c \,\mathrm{Tr}(\hat{\sigma}_{ge}L[\delta\hat{\rho}]). \tag{A.2}$$

We look to solve for $L[\delta\alpha]$ and need the Laplace transform of Eq. (3.11) which is

$$L[\delta\hat{\rho}] = W^{-1}(s)\delta\hat{\rho}(0) - ig_c L[\delta\alpha^*]W^{-1}(s)[\hat{\sigma}_{ge},\hat{\rho}_0] - ig_c L[\delta\alpha]W^{-1}(s)[\hat{\sigma}_{eg},\hat{\rho}_0], \tag{A.3}$$

where $W(s)^{-1}$ is the inverse of the operator given in Eq. (3.19). Then after substituting Eq. (A.3) into Eq. (A.2), we arrive at

$$\begin{aligned} L[\delta\alpha] =& s^{-1}\Big[\delta\alpha(0) - \left(i\Delta_c' + \frac{\kappa}{2}\right)L[\delta\alpha] - iNg_c Z(s) - Ng_c^2 L[\delta\alpha^*]X(s) \\ & - Ng_c^2 L[\delta\alpha]Y(s)\Big]. \end{aligned} \tag{A.4}$$

Eq.(A.4) can be expressed in terms of a matrix-vector product

$$\vec{\mathbf{b}} = D(s)^{-1}\mathrm{adj}(\mathbf{C}(s))\vec{\mathbf{x}}, \tag{A.5}$$

where adj ($\mathbf{C}$) is the adjugate of matrix $\mathbf{C}$. The elements of $\mathbf{C}$ are given in Eq. (3.16) and vectors $\vec{\mathbf{b}}$ and $\vec{\mathbf{x}}$ are defined as

$$\vec{\mathbf{b}} = \begin{pmatrix} L[\delta\alpha] \\ L[\delta\alpha^*] \end{pmatrix}, \quad \vec{\mathbf{x}} = \begin{pmatrix} \delta\alpha(0) - iNg_c Z(s) \\ \delta\alpha^*(0) + iNg_c Z^*(s) \end{pmatrix}; \tag{A.6}$$

the dispersion relation is then

$$D(s) = \det\left[\mathbf{C}(s)\right]. \tag{A.7}$$

The dynamics of $\delta\alpha$ are determined by the value largest real part of s for which $D(s)$ is not invertible (i.e., when $D(s) = 0$).

Appendix B

U(1) Transformation Derivation

This appendix is to verify that Eq.(3.30) possesses a component that is $U(1)$ symmetric. We look to see whether the field α_{-1} is invariant under the transformation

$$\alpha_{-1} \mapsto \alpha_{-1} e^{-i\varphi}, \quad \hat{\rho}_{-1} \mapsto e^{-i\varphi\hat{\sigma}_{ee}} \hat{\rho}_{-1} e^{i\varphi\hat{\sigma}_{ee}}, \tag{B.1}$$

with arbitrary phase φ. This transformation indicates we are moving into the interaction picture defined by $H^{'} = \hbar\hat{\sigma}_{ee}$, which means we are changing the relative phase between the $|g\rangle \leftrightarrow |e\rangle$ transition and field. By applying Eq. (B.1) to Eq. (3.30) we get

$$\alpha_{-1} e^{-i\varphi} = \frac{-iNg_c \operatorname{Tr}\big(\hat{\sigma}_{ge} e^{-i\varphi\hat{\sigma}_{ee}} \hat{\rho}_{-1} e^{i\varphi\hat{\sigma}_{ee}}\big)}{i(\Delta_c^{'} + \omega n) + \frac{\kappa}{2}}. \tag{B.2}$$

We first calculate the exponential terms containing an operator by performing a Taylor expansion

$$\begin{aligned} e^{-i\varphi\hat{\sigma}_{ee}} &= \sum_{k=0}^{\infty} \frac{(-i\varphi\hat{\sigma}_{ee})^k}{k!}, \\ &= \hat{\mathbb{I}} + \sum_{k=1}^{\infty} \frac{(-i\varphi)^k}{k!} \hat{\sigma}_{ee} + \hat{\sigma}_{ee} - \hat{\sigma}_{ee}, \\ &= \hat{\mathbb{I}} + \sum_{k=0}^{\infty} \frac{(-i\varphi)^k}{k!} \hat{\sigma}_{ee} - \hat{\sigma}_{ee}, \\ &= \hat{\mathbb{I}} + e^{-i\varphi}\hat{\sigma}_{ee} - \hat{\sigma}_{ee}, \end{aligned} \tag{B.3}$$

where we have added a zero to obtain a more convenient form of the exponential term. Then substituting Eq. (B.3) into the trace we get

$$\operatorname{Tr}\Big(\hat{\sigma}_{ge} e^{-i\varphi\hat{\sigma}_{ee}} \hat{\rho}_{-1} e^{i\varphi\hat{\sigma}_{ee}}\Big) = \operatorname{Tr}\Big(\hat{\sigma}_{ge}(\hat{\mathbb{I}} + e^{-i\varphi}\hat{\sigma}_{ee} - \hat{\sigma}_{ee})\hat{\rho}_{-1}(\hat{\mathbb{I}} + e^{i\varphi}\hat{\sigma}_{ee} - \hat{\sigma}_{ee})\Big). \tag{B.4}$$

Next, using the fact that the trace is invariant under cyclic permutations (i.e., $\mathrm{Tr}(\mathbf{ABC}) = \mathrm{Tr}(\mathbf{BCA}) = \mathrm{Tr}(\mathbf{CAB})$) Eq. (B.4) simplies to

$$\mathrm{Tr}\big(\hat{\sigma}_{ge}e^{-i\varphi}\hat{\rho}_{-1}\big) = e^{-i\varphi}\,\mathrm{Tr}(\hat{\sigma}_{ge}\hat{\rho}_{-1}), \tag{B.5}$$

where we have also used the property $\mathrm{Tr}(c\mathbf{A}) = c\,\mathrm{Tr}(\mathbf{A})$. Eq. (B.2) then becomes

$$\alpha_{-1}e^{-i\varphi} = e^{-i\varphi}\frac{-iNg_c\,\mathrm{Tr}(\hat{\sigma}_{ge}\hat{\rho}_{-1})}{i(\Delta_c' + \omega n) + \frac{\kappa}{2}}, \tag{B.6}$$

and is clear that Eq. (3.30) is invariant under this $U(1)$ transformation. As previously stated this indicates the field α_{-1} is not locked to the phase of an external driving laser.

Appendix C

Additional Mean-Field Results

This appendix shows an extension of the mean-field formalism where we simulate our mean-field equations with a noisy classical field. We derive our equations of motion by using the many-body master equation Eq. (2.36), then for a general time-independent operator $\hat{O}$, we write

$$\begin{aligned}\partial_t \left\langle \hat{O} \right\rangle &= \mathrm{Tr}\left[\hat{O}\partial_t\hat{\rho}\right] = \mathrm{Tr}\left[\frac{1}{i\hbar}\left(\hat{O}\hat{H}\hat{\rho} - \hat{O}\hat{\rho}\hat{H}\right) + \sum_k \left(\hat{O}\hat{J}_k\hat{\rho}\hat{J}_k^\dagger - \frac{1}{2}\hat{O}\hat{J}_k^\dagger\hat{J}_k\hat{\rho} - \frac{1}{2}\hat{O}\hat{\rho}\hat{J}_k^\dagger\hat{J}_k\right)\right] \\ &= \mathrm{Tr}\left[\left(\frac{1}{i\hbar}\left(\hat{O}\hat{H} - \hat{H}\hat{O}\right) + \sum_k \left(\hat{J}_k^\dagger\hat{O}\hat{J}_k - \frac{1}{2}\hat{O}\hat{J}_k^\dagger\hat{J}_k - \frac{1}{2}\hat{J}_k^\dagger\hat{J}_k\hat{O}\right)\right)\hat{\rho}\right] \\ &= \left\langle \frac{1}{i\hbar}\left[\hat{O},\hat{H}\right] + \sum_k \left(\hat{J}_k^\dagger\hat{O}\hat{J}_k - \frac{1}{2}\{\hat{J}_k^\dagger\hat{J}_k,\hat{O}\}\right)\right\rangle = \left\langle \hat{\mathcal{L}}^\ddagger[\hat{O}]\right\rangle,\end{aligned} \tag{C.1}$$

where we have used the cyclic property of the trace and $\{\hat{A},\hat{B}\} = \hat{A}\hat{B}+\hat{B}\hat{A}$ is the anti-commutator. This is the quantum Heisenberg-Langevin equation with zero average noise, given by the dual of the Liouvillian superoperator operating on $\hat{O}$. We now choose to treat the field as a noisy complex number with mean value $\alpha(t) = (\alpha_x - i\alpha_y)/2$ and small fluctuations $\delta\alpha(t)$. The complex field $\alpha(t)$ can be separated into real and imaginary components, otherwise referred to as quadratures and are defined as

$$\alpha_x = \left\langle \hat{c} + \hat{c}^\dagger \right\rangle, \quad \alpha_y = i\left\langle \hat{c} - \hat{c}^\dagger \right\rangle, \tag{C.2}$$

according to symmetric ordering. Substituting $\alpha(t)$ into the mean-field master equation Eq. (3.5) and averaging over the field quadratures we get

$$\partial_t\hat{\rho}_1 = \hat{\mathcal{L}}_A\hat{\rho}_1 - i\left\langle \frac{g}{2}\left[\left\langle \hat{\sigma}^{(1)}_{x,ge}\right\rangle,\hat{\rho}_1\right]\right\rangle_{\alpha_x} + i\left\langle \frac{g}{2}\left[\left\langle \hat{\sigma}^{(1)}_{y,ge}\right\rangle,\hat{\rho}_1\right]\right\rangle_{\alpha_y}. \tag{C.3}$$

where $\hat{\rho}_1 = \mathrm{Tr}_F\left[\hat{\rho}_{AF}\right]$ is the reduced atomic density operator, $\mathrm{Tr}_X[\cdot]$ is the partial trace over the subspace X, $\langle\cdot\rangle_Y$ denotes an average over Y, and

$$\hat{\sigma}^{(j)}_{x,ik} = \hat{\sigma}^{(j)}_{ik} + \hat{\sigma}^{(j)}_{ki}, \quad \hat{\sigma}^{(j)}_{y,ik} = i\left(\hat{\sigma}^{(j)}_{ki} - \hat{\sigma}^{(j)}_{ik}\right), \quad \hat{\sigma}^{(j)}_{z,ik} = \hat{\sigma}^{(j)}_{kk} - \hat{\sigma}^{(j)}_{ii}, \tag{C.4}$$

are the x, y, z Pauli operators for the $|i\rangle \leftrightarrow |k\rangle$ transition of spin j with $E_k > E_i$. We can now write the equation of motion for the field as

$$\partial_t \alpha(t) = -i\Delta'_c \alpha(t) - iNg_c\left\langle \hat{\sigma}^{(1)}_{ge}\right\rangle - \frac{\kappa}{2}\alpha(t), \tag{C.5}$$

such that

$$\partial_t \alpha_x(t) = -\Delta'_c \alpha_y(t) + Ng_c\left\langle \hat{\sigma}^{(1)}_{y,ge}\right\rangle - \frac{\kappa}{2}\alpha_x(t), \tag{C.6}$$

and

$$\partial_t \alpha_y(t) = \Delta'_c \alpha_x(t) + Ng_c\left\langle \hat{\sigma}^{(1)}_{x,ge}\right\rangle - \frac{\kappa}{2}\alpha_y(t). \tag{C.7}$$

We randomize the noise in our simulations by choosing random numbers r_x and r_y after a full RK4 step from a normal distribution centered at zero and then updating the field quadratures by

$$\alpha_x(t+dt) = \partial_t \alpha_x(t) + r_x\sqrt{\kappa dt}, \quad \alpha_y(t+dt) = \partial_t \alpha_y(t) + r_y\sqrt{\kappa dt}, \tag{C.8}$$

where dt is the time step and κ is the cavity decay rate. We then estimate the field intensity by

$$\left\langle \hat{c}^\dagger \hat{c}\right\rangle \approx |\alpha|^2 \approx \frac{(\alpha_x^2 + \alpha_y^2) - 2}{4}. \tag{C.9}$$

In Fig. C.1 we look to compare the steady-state intensity of the noisy mean-field and second-order cumulant results. As we can see, the steady-state values are in good agreement. However, the noisy mean-field simulations are much more computationally intensive and yield the same averaged value as the mean-field without noise results. For this reason we chose to perform our simulations without noise to have faster simulation times, yet still obtaining the same averaged results.

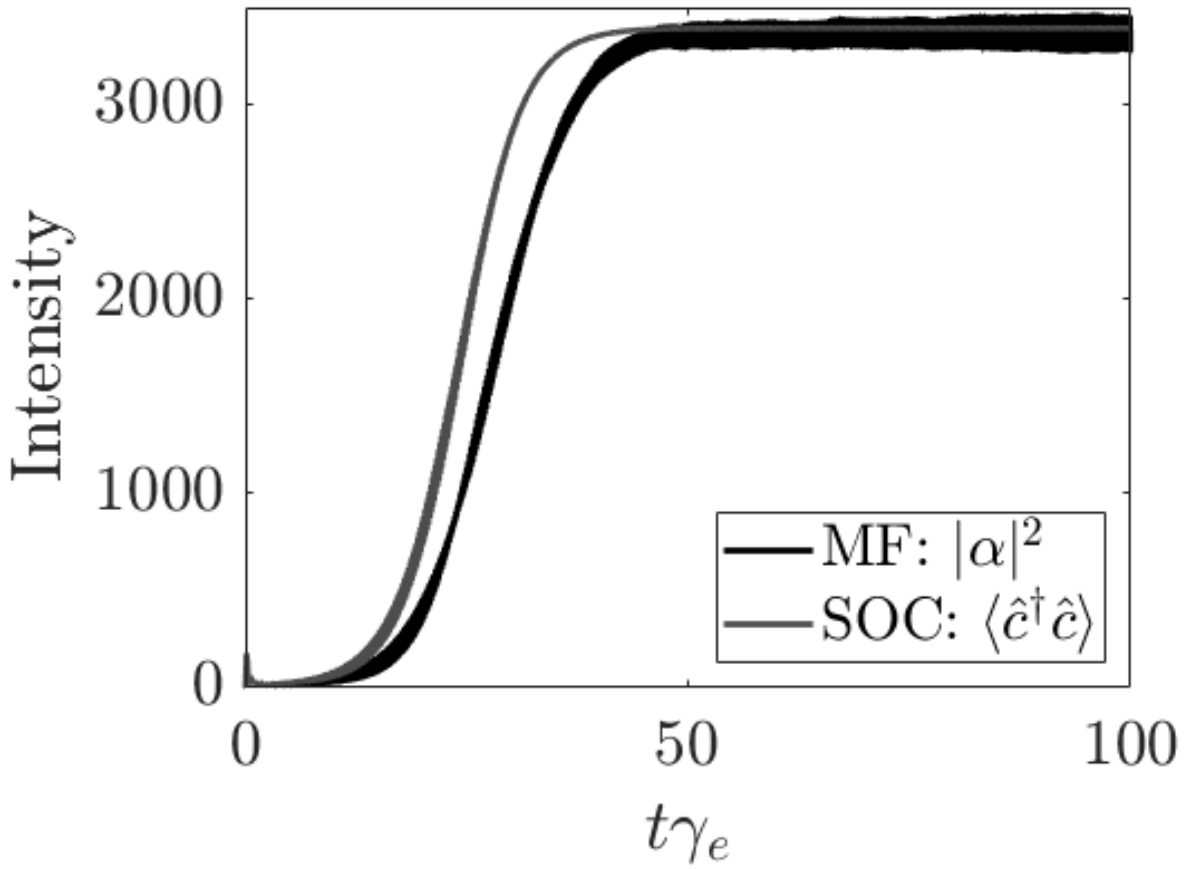

Figure C.1: Dynamical comparison of the intensity $|\alpha|^2$ for mean-field with noise averaged over 100 simulations (MF, black curve) and $\langle \hat{c}^\dagger \hat{c} \rangle$ for second-order cumulants (SOC, dark gray curve). The parameters are the same as in Fig. 3.2 with $N = 20000$ and $\Delta_p = 0$.